Development of high-resolution multi-scale modelling system for simulation of coastal-fluvial urban flooding

Joanne Comer[1], Agnieszka Indiana Olbert[1], Stephen Nash[1], Michael Hartnett[1]

[1]Civil Engineering, College of Engineering and Informatics, Ryan Institute, National University of Ireland, Galway, University Road, Galway, Ireland

Correspondence to: Dr. Agnieszka Indiana Olbert (indiana.olbert@nuigalway.ie)

Abstract. Urban developments in coastal zones are often exposed to natural hazards such as flooding. In this research, a state-of-the-art, multi-scale nested flood (MSN_Flood) model is applied to simulate complex coastal-fluvial urban flooding due to combined effects of tides, surges and river discharges. Cork City on Ireland's southwest coast is a study case. The flood modelling system comprises of a cascade of four dynamically linked models that resolve the hydrodynamics of Cork Harbour and/or its sub region at four scales 90m, 30m, 6m and 2m.

Results demonstrate that the internalisation of the nested boundary through a use of ghost cells combined with a tailored adaptive interpolation technique creates a highly dynamic moving boundary that permits flooding and drying of the nested boundary. This novel feature of MSN_Flood provides a high degree of choice regarding the location of the boundaries to the nested domain and therefore flexibility in model application. The nested MSN_Flood model through dynamic downscaling facilitates significant improvements in accuracy of model output without incurring the computational expense of high spatial resolution over the entire model domain. The urban flood model provides full characteristics of water levels and flow regimes necessary for flood hazard identification and flood risk assessment.

Keywords: Urban flooding; Coastal flooding; Fluvial flooding; Hydrodynamic modelling; Nesting; Moving boundary

1 Introduction

Low lying developments in coastal zones are exposed to natural hazards such as storm surges, waves, tsunamis and/or high river flows which can lead to significant flooding. Coastal flooding can result in substantial economic and social impacts including loss of life, damage to property and disruption of essential services (Brown et al., 2007).

Coastal flooding results from a rise of sea water level above normal predicted tide level. On the European Continental Shelf, coastal flooding is associated with storms generated in the Atlantic Ocean that travel through, or in proximity to, the shelf. Storm surges are important consequences of these storms – a temporary water setup resulting from synoptic variation of atmospheric pressure and strong winds blowing towards the shelf causing water to pile up against the coast. Surge physics is well understood in principle (Ponte, 1994); the mechanism of its propagation on the European continental shelf as a response to meteorological conditions (wind stress and atmospheric pressure signal separate) has been explained by Olbert and Hartnett (2010).

Flood dynamics due to a combination of multiple process drivers such as tides, surges and river inflows and their interactions is extremely difficult to understand using non-modelling methods (Robins et al., 2011). In recent years the amount of flood modelling work has risen dramatically. Yet the modelling still encounters various problems of which input data such as topography (Mason et al, 2007; Smith, 2002), mesh resolution (Sanders et al, 2010; Fewtrell, 2011; Horritt et al, 2006; Yu and Lane, 2006), bottom roughness (Mason et al., 2003; Horritt, 2000) or modelling framework (Hunter et al., 2008) are of greatest challenge. So far, one of the main issues hampering research into coastal flood modelling has been the lack of topographic data of sufficiently high resolution and accuracy along with highly resolvable efficient models. In the past decade, high resolution topographic has become more available with airborne scanning laser altimetry (LIDAR) technology (Gomes-Pereira and Wicherson, 1999) providing high resolution digital surface maps that can be used as model bathymetry (Marks and Bates, 2000). Although there are still problems with mapping urban areas and considerable post-processing is necessary to extract digital terrain model from digital surface model (Mason at al., 2007), the hydraulic/hydrodynamic models developed using LIDAR data allow them to numerically propagate surge and tidal waves into coastal areas. Model accuracy and computational cost are still issues to be addressed.

The most common and simple approach to the modelling of coastal flooding in urban areas is to link (externally or dynamically) longitudinal 1D or latterly averaged 2D hydraulic models with coastal models (e.g. Formaggia, 2001; Chen, 2007; Brown et al., 2007). Such a set up has two significant drawbacks. Firstly, 1D/2D hydraulic models work with the assumption that the lateral variations in velocity magnitudes are small, while in reality many coastal floodplains (e.g. urban areas) contain channels that have a significant influence on the development of inundation by providing routes along which storm surges propagate inland (Bates et al., 2005) and therefore may lead to misrepresentation of localized flooding (Cook and Merwade, 2009; Mark et al, 2004). Secondly, numerical errors may be introduced when linking different models with different dimensions resulting from poor conservation of momentum (Yang et al., 2012). There is evidence of proven difficulty in ensuring that each model interprets the model inputs and boundary conditions in the same way (Hunter et al. 2008; Pender and Neelz, 2010).

These problems may be overcome by application of a single hydrodynamic model to both coastal waters and coastal floodplains. Although such a model would allow smooth transition of the model solution between coastal waters and floodplains, the full solution at scales appropriate for flood inundation would incur a significant computational cost. On one hand, such models need to extend far enough offshore to capture the development and propagation of surge and to resolve the nonlinear shallow water dynamics (interactions between tides, surges and waves) at a resolution that is commensurate with flow features. On the other hand the model needs to include upstream river channels, tidal flats, low-lying land and urban areas which are susceptible to flooding at very fine resolution. This often results in a model setup that requires a large computational domain of which the area of particular interest (such as floodplains here) comprises only a small percentage. For structured grid models such requirements are often cost prohibitive and the alternative is to use lower resolution at the expense of accuracy. This means that model discretization is performed at scales well below those achievable with LIDAR data (the level of individual buildings in the case of urban flooding) meaning the highly-resolved LIDAR data are not being optimally used (McMillian and Brasington, 2007). Some quite successful attempts have been made using unstructured-grid models allowing selective grid refinement (e.g. Yang et al., 2012; Robins et al., 2011); however, the computational demand of these models is high. A relatively new approach to address this problem in high-resolution flood modelling makes use of continuing advances in computational resources through numerical domain decomposition and multi core architecture runs (Sanders et al., 2010). This method, however, requires substantial computational resources not commonly available yet.

In reality the modelling of coastal flooding (particularly in an urban environment) is a multi-scale problem that requires accurate solution at various scales ranging from coastal sea or estuary scale down to a dense street network of the inundated urban area. In the case of single rectilinear grid models, which are still the most commonly used hydrodynamic models, this spatial resolution problem may be overcome by grid nesting; this involves embedding higher resolution grids within a lower resolution global large-scale grid model. Such a solution allows users to specify high resolution in a sub-region of the model domain without incurring the computational expense of fine resolution over the entire domain. Nonetheless, the nested model for simulation of floodplains must be very carefully chosen due to the flooding and drying properties of such zones; most nested models developed to date do not incorporate flooding and drying as they have been developed specifically for large-scale application where this phenomenon is not important (e.g. ROMS, Haidvogel et al., 2008) or, even if they incorporate flooding and drying such as Mike21 (DHI Software, 2001) flooding and drying of open boundaries is prohibited. This problem has been recently resolved in the multi-scale nested flood (MSN_Flood) model of Nash and Hartnett (2010) which allows flooding and drying both within the domain and along boundaries, while maintaining accuracy and computational efficiency. This model is ideally suited for high-resolution modelling of urban flooding and, therefore, has been adopted for further development in this research.

In this context, the authors present in this paper for the first time the application of the state-of-the-art flood model, MSN_Flood, to complex coastal-fluvial urban flooding in the estuary-lying Cork City which is subject to the combined effects of tides, surges and river discharges. The primary objectives of this paper then are to present the development of this model and to critically examine its capability to forecast/hindcast the urban inundation. It will be demonstrated in this paper that through the novel solution to the nested boundary, the so-called moving boundary, the nested model allows simulation of the propagation of open sea conditions up to the tidally active river upstream as well as rural and urban floodplains in a computationally efficient manner without compromising model accuracy or stability.

The modelling framework proposed in this research comprises of a cascade of multiple nested models that dynamically downscale large scale, coastal sea processes to the fine resolution scale of urban environments. MSN_Flood was applied to the area of Cork City, Ireland, and its coastal floodplains; Cork City is frequently subject to coastal-fluvial flooding. An extreme flood event of November 2009 that resulted in approximately €100 million of flood damage in the city and its surrounds was chosen as a test case. The main features of this accurate and efficient hydraulic modelling are illustrated through the Cork City application. In particular, wetting and drying routine, computational efficiency and accuracy of simulated water elevations and velocity fields are subject to in-depth analysis in this research.

This paper is organized as follows: section 1 describes the motivation for this research and related work; section 2 describes modelling, model setup and datasets; section 3 presents and compares numerical model results with observed datasets; section 4 discusses the advantages the MSN_Flood modelling system, and finally section 5 contains conclusions from the research.

2 Methodology

In this section a modelling system for coastal flood inundation is described along with the datasets and model setup for the Cork City flood event.

2.1 Modelling framework

Many flood inundation events in urban environments have been modelled using simple hydraulic models, such as HEC-RAS (Pappenberger et al., 2005) or LISFLOOD-FP (Bates and De Roo, 2000), incapable of simulating flood water velocities required for accurate determination of flood wave propagation routes and assessment of risks associated with a certain flood flow magnitude. A more realistic analysis can be achieved using a hydrodynamic model that resolves both the continuity and momentum equations throughout the entire domain.

Here, the MSN_Flood model was applied to Cork City using a cascade of four nested grids to describe hydrodynamics at various scales with particular interest in water elevations and velocity fields over the inundated area. This nested model facilitates the refinement of spatial resolution in Cork Harbour from 90 m at the outer reaches of the harbour down to 2 m in the streets of Cork City.

2.2 Hydrodynamics

MSN is a two-dimensional, depth-averaged, finite difference model and its solver is based on the alternate direction implicit (ADI) solver developed by Falconer (1984) (Lin and Falconer, 1997; Nash and Hartnett, 2010). The governing differential equations used in the model to determine the water elevation and depth integrated velocity fields in the horizontal plane are based on integrating the three-dimensional continuity and Navier-Stokes equations over the water column depth. Assuming vertical accelerations are negligible compared with gravity and that the Reynolds stresses in the vertical plane can be represented by a Boussinesq approximation, then the depth integrated continuity and x-direction momentum equations are of the following form (Falconer and Chen, 1991):

Continuity equation

$$\frac{\partial \zeta}{\partial t} + \frac{\partial q_x}{\partial x} + \frac{\partial q_y}{\partial y} = 0 \quad (1)$$

Momentum equation in x-direction

$$\frac{\partial q_x}{\partial t} + \beta\left[\frac{\partial U q_x}{\partial x} + \frac{\partial U q_y}{\partial y}\right] = f q_y - gH\frac{\partial \zeta}{\partial x} + \frac{\rho_a C^* W_x (W_x{}^2 + W_y{}^2)^{1/2}}{\rho} \quad (2)$$

$$- \frac{gU(U^2+V^2)^{1/2}}{C^2} + 2\frac{\partial}{\partial x}\left[\varepsilon H \frac{\partial U}{\partial x}\right] + \frac{\partial}{\partial y}\left[\varepsilon H\left[\frac{\partial U}{\partial y} + \frac{\partial V}{\partial x}\right]\right]$$

where, t = time

U,V = depth-averaged velocity components in the x,y directions

q_x,q_y = depth integrated volumetric flux components in the x,y directions ($q_x=UH$, $q_y=VH$)

H = total water depth

β = momentum correction factor for non-uniform vertical velocity profile

f = Coriolis parameter (= $2\omega Sin\ \phi$, where ω = angular velocity of the earth's rotation and ϕ = geographical latitude)

g = gravitational acceleration

ρ_a, ρ = air and fluid densities respectively

C^* = air-water interfacial resistance coefficient

W_x,W_y = wind velocity components in x,y directions

C = Chezy bed roughness coefficient

ε = depth mean eddy viscosity

2.3 Nesting structure and procedure

MSN_Flood consists of one outer coarse grid called the parent grid (PG) into which one or more inner fine grids (child grids, CG) are one-way nested. The model also enables multiple nesting such that a child grid may also be a parent to another child. In this way, multi-scale nesting can be specified enabling high spatial resolution in areas of interest. PG and CG models are dynamically coupled and synchronous. An overview of the nesting procedure is schematically presented in Fig. 1. As can be seen, the time integration is a bottom-up approach where PG can be advanced in time only when all of its children are integrated to the parent current time. The ADI solution technique to solve the governing continuity and momentum equations requires the sub-division of each timestep into two half-timesteps. The nesting procedure, for each nesting level, is summarized in the following 5 steps:

1. integrate outermost parent grid one timestep ($t+\Delta t_p$)
2. extract parent grid data and interpolate (spatially and temporally) along child grid boundary to next time levels of child grid ($t+½\Delta t_c$) and ($t+\Delta t_c$)
3. integrate child grid one timestep ($t+\Delta t_c$)
4. repeat Steps 2 and 3 so that the child grid is synchronised to the current timestep of parent grid ($t+\Delta t_p$)
5. return to Step 1 and continue.

The nesting procedure is similar in principle to other nested models (Holt et al., 2009; Korres and Lascaratos, 2003; Nittis et al., 2006) but the uniqueness of MSN_Flood is a novel approach to boundary formulation through an incorporation of ghost cells in a manner that the nested boundary operates as an internal boundary. Ghost cells (GC) are specified adjacent to nested boundaries so that the boundary configuration consist of two rows/columns of CG cells: internal boundary cells and the adjacent exterior ghost cells. A schematic of the general configuration of the nested boundary is shown in Fig. 2. In this internal boundary approach, PG boundary data is specified to both the ghost cells outside the CG domain and to the internal boundary cells allowing the governing equations of motion at the internal boundary grid cells to be formulated and solved in the same way as interior grid cells. This enables accurate specification and conservation of incoming fluxes of mass and momentum along the boundaries of the nests. To demonstrate benefits of this approach the finite difference formulation for the advective term in the momentum equation, which is key to momentum conservation, at boundary cells becomes:

$$\frac{\partial U q_x}{\partial x} = \left[\frac{[U(x+\Delta x,y)+U(x,y)]}{2} \cdot \frac{[q_x(x+\Delta x,y)+q_x(x,y)]}{2} \right. \tag{3}$$

$$\left. - \frac{[U(x,y)+U(x-\Delta x,y)]}{2} \cdot \frac{[q_x(x,y)+q_x(x-\Delta x,y)]}{2} \right]$$

For comparison, in a boundary formulation without ghost cells, the derivative $\partial Uq_x / \partial x$ would be set to zero as ghost cell grid points $U(x+\Delta x, y)$ or $U(x-\Delta x, y)$ would not exist, therefore momentum would not be conserved between parent grid and child grid.

An important feature of the nesting approach in MSN_Flood is the implementation of moving boundaries along the boundary of the nested domains. The flooding and drying routine originally developed in by Falconer and Chen (1991) is implemented in MSN_Flood; this boundary formulation allows the model to be applied to areas of inter-tidal zone or coastal flooding where there is typically a considerable degree of alternate flooding and drying throughout the domain. The flooding and drying routine by Falconer and Chen has been extensively tested in laboratory conditions and natural waterbodies and shown to be stable and robust. However, when the nested boundary was subject to flooding and drying, despite the overall improvement in mass and momentum conservation along the nested boundary, significant errors were found to occur near the boundary in areas of flooding and drying. This problem was overcome by implementation of an adaptive interpolation scheme which uses linear interpolation or zeroth-order interpolation depending on the status (wet or dry) and the configuration of parent grids along the boundary interface. More details of the method can be found in Nash (2010). This adaptive interpolation in combination with ghost cell and internal boundary formulation ensures the stable flooding and drying of boundary cells.

The ghost cell formulation of the boundary was found to significantly reduce boundary formulation errors, one of three error sources in nested models as classified by Nash and Hartnett (2010). Boundary formulation errors arise from simplification of mathematical formulation of the governing equations of motion at open boundary grid cells. Two other sources of errors at the boundary interface are boundary specification errors and boundary operation errors. While the former errors arise from incorrect boundary data, and can be minimised by locating nested boundary in areas of high PG accuracy, boundary operator errors result from the use of an inadequate interpolation schemes and/or boundary condition for prescribing PG data to the CG boundary and are more challenging to reduce. During the course of model developments various interpolation schemes were tested including a zeroth order scheme, a linear scheme, a mass-conserving quadratic scheme and an inverse distance weighted scheme. The linear interpolation was found to be most accurate in both time and space and therefore was implemented in the model (Nash, 2010). With regards to the boundary conditions, three different types of boundary conditions were tested, namely: Dirichlet condition, flow relaxation condition and radiation condition. Extensive numerical testing showed that the most stable and accurate model solution could be achieved by implementing the Dirichlet boundary condition. Accuracies of various interpolation and boundary condition schemes were analysed and compared in Nash and Hartnett (2014).

Reduction in boundary errors due to the accurate development of boundary operators and more accurate mathematical formulation of the nested boundary yielded significant improvements in conservation of mass and momentum between parent and child grids. This in turn improved model stability at the nested boundary and CG accuracy. These features make MSN_Flood highly applicable to modelling complex coastal flooding events as in the current test case, where the nested boundary is located in the flooding and drying zone, and therefore its length changes dynamically throughout the flooding event. This non-continuous moving boundary feature is the subject of in-depth investigation in this research.

2.4 Study area description and model setup

Cork Harbour, in the southwest of Ireland, is a shallow (average depth 8.4 m) meso-tidal estuary with typical spring tide ranges of 4.2m. Return levels of tides for 2- and 100-year return periods are 4.45 m and 4.52 m above chart datum, respectively, while surge residual return levels for the same return periods are 0.56 m and 0.85 m, respectively (Olbert and Hartnett, 2013). The Cork Harbour domain is presented in Fig. 3. Cork City is a densely populated urban area of approximately 120,000 people, located at the mouth of the River Lee which drains into Cork Harbour. Tidal components of flooding in Cork City are due to combinations of high astronomical tides and storm surges generated in the open ocean and propagating into the Harbour and throughout the city streets. The River Lee corridor flows from west to east along the post-glacial valley into the Lee proper, through Cork City, into Lough Mahon, Cork Harbour and south into Atlantic Ocean. In the city, the River Lee bifurcates into the north and south channels around the Mardyke area and merges again at the eastern edge of the city. The river flows for 2- and 100-year return periods are 208.6 and 307.7 m^3/s, respectively (Halcrow, 2008). Sea water intrusion up the river is bounded by a weir located 8km upstream from the river mouth.

MSN_Flood was used in this research to develop a coastal-urban hydraulic model capable of simulating fluvial and coastal flooding in the Cork City. The model grid needs to be setup to include not only river channel and urban floodplains but also offshore waters necessary to resolve the non-linear hydrodynamics. The Cork Harbour/City model is therefore configured as a four level cascade of dynamically linked nested grids that resolve the hydrodynamics of the region at spatial scales of 90m, 30m, 6m and 2m. Each coarser grid provides boundary conditions to the next finer grid, i.e. the 90m grid provides boundary conditions to the30m grid and the 30 m grid provides boundary conditions to the 6m grid, etc. Fig. 4a illustrates the extent of each grid and the nesting structure, while Fig. 4b shows details of the high resolution 6m grid and the 2m urban flood grid.

The parent grid (PG90) representing the full domain of Cork Harbour was resolved at a grid spacing of 90m. At 3:1 nesting ratio, the first child grid (CG30), completely embedded within the parent model domain, has a grid spacing of 30m. The CG30 model provides boundary conditions to a 6m grid (CG06) at a 5:1 nesting ratio. The domains of CG30 and CG06 models only partially overlap. Water elevations computed on CG30 are passed to the eastern boundary of CG06 while River Lee flow data are specified at the western boundary of CG06. Finally, the ultra-high resolution 2m child grid (CG02) is entirely embedded within CG06 and is used to simulate urban flooding of Cork City. The nesting ratios of 3:1 and 5:1 used in this setup are in line with nesting ratios used in other studies (e.g. Spall and Holland, 1991). Configurations of the nested models are summarized in Table 1.

Open boundary conditions to the MSN_Flood parent grid, PG90, are provided as total water elevations containing tidal and surge signals extracted from an ocean model of the North East Atlantic (Olbert and Hartnett, 2010). The surface boundary of the MSN_Flood model is forced by 10-m wind fields and mean sea level atmospheric pressure obtained from the regional analysis ERA-40 model (Uppala et al., 2005) and operational model first-guess dataset (Simmons et al., 1989). River Lee discharges from gauge station 19011 were provided by Office of Public Works (OPW), Ireland. Admiralty Chart data were used to develop the bathymetric model of Cork Harbour, while high resolution LiDAR data provided by the OPW were used to construct the high resolution urban digital bathymetric model. The channel of the River Lee was included in the model based on cross-sectional survey data also provided by the OPW from an extensive survey of the River Lee catchment in 2008.

2.5 Verification

The numerical model skill was assessed by statistically comparing observations and model solutions. Following statistical measures were used:

- root mean square error

$$RMSE = \left[\frac{1}{N} \sum_{n=1}^{N} \left(Y_n - X_n \right)^2 \right]^{1/2} \qquad (4)$$

- root mean square difference between model and observations

$$RMSdiff = \left[\frac{1}{N}\sum_{n=1}^{N}(Y_n)^2\right]^{1/2} - \left[\frac{1}{N}\sum_{n=1}^{N}(X_n)^2\right]^{1/2} \quad (5)$$

- centered root mean square difference

$$RMSD = \left[\frac{1}{N}\sum_{n=1}^{N}\left(\left(Y_n - \overline{Y}\right) - \left(X_n - \overline{X}\right)\right)^2\right]^{1/2} \quad (6)$$

where $\overline{X}$ and $\overline{Y}$ are the mean values of variables X and Y, respectively, for N observations. These measures were also used to inter-compare time-series of models of different resolutions.

The spatially comparative measures between various models are based on spatial distribution of errors between fine and coarse resolution models and are quantified using following expressions:

- tidally-averaged relative errors

$$RE_T = \frac{\sum_{n=1}^{N}\left|Y_n - X_n\right|}{\sum_{n=1}^{N}\left|X_n\right|} \cdot 100 \quad (7)$$

- domain-averaged relative error

$$RE_D = \frac{RE_T}{M} \quad (8)$$

- absolute error

$$AE_T = \frac{\sum_{n=1}^{N}\left|Y_n - X_n\right|}{N} \quad (9)$$

- relative difference

$$RD = \frac{\left|X_n - Y_n\right|}{X_n} \quad (10)$$

where X and Y are higher and coarser resolution solutions, respectively, n is the output time over a tidal cycle, N=25 is the total number of tidal cycles and M is the number of discrete points in space.

3 Results

Showcasing the capability of the multilevel nesting integrated system to accurately simulate the extent and level of urban flooding is central to this research. MSN_Flood has been extensively tested in both laboratory settings (against physical tidal models) and natural open harbours. In this research, a comprehensive validation of the model in a coastal flood application to Cork Harbour and the urban environment of Cork City is presented. Initial evaluation of model accuracy is carried out at each of the four levels of nesting; both modelled water elevations and velocities are compared to available field data. The assessment of the model skill in simulation of urban flooding is carried out for the November 2009 coastal-fluvial flooding of Cork City. In this application, the city streets and open areas are treated as hydraulics channels and plains that can be inundated depending on the tide, surge and fluvial conditions. This is a highly complex hydrodynamic region to model and, therefore, represents a robust test of the model.

3.1 Validation of the nesting procedure

3.1.1 PG90 model

Firstly, the performance of the low resolution 90m parent grid (PG90) model was assessed. Figure 5 compares current velocities simulated by the PG90 model with measured data at Passage West in Cork Harbour over a spring tidal cycle (see Fig. 3 for point P1 location). Results show that although pattern of currents through flood and ebb conditions are relatively well predicted, the slack water conditions, where velocities are generally smaller, are not reproduced correctly by the PG90 model. A higher resolution single grid (SG30) model at 30m grid spacing was developed to test the accuracy of PG90. The same domain extents (Fig. 4) and the same physical conditions were specified to the SG30 and PG90 models. As shown in Fig. 5 an increased resolution of the model significantly improves model predictions throughout the tidal cycle and particularly during periods of slack water.

The spatial distribution of PG model error was quantified by calculating the tidally-averaged relative errors RE_T expressing a percentage error in a PG solution relative to a higher resolution SG reference solution (Equation 7). Figure 6 shows the distribution of RE_T in PG velocities in Cork Harbour; it can be seen that the errors generated by the PG model are well over 30% at certain locations within the harbour (harbour entrance, along the coastline, narrow channels and estuaries) so increasing the resolution from 90m to 30m leads to significant reduction in the error. However, improvements in accuracy due to higher spatial resolution come at a high computational cost which for the SG model (80min for 50hrs run) is nine times that of the PG model (9min for 50 hrs run). The use of nested model is then a justifiable and favourable solution.

In the course of extensive validation, the timeseries of PG90 and SG30 were also inter-compared. Figure 7 shows water elevations and current velocities in Lough Mahon (see Fig. 3 for point C1 location). Water elevations computed by both models are in very good agreement. In contrast, current velocities are significantly overpredicted by the PG90 model. Linear regression of current speeds of PG90 against SG30 solution is shown in Fig. 8. As can be seen from this figure the correlation coefficient between PG90 and SG30 is 0.89 while slope and intercept are m=1.24 and c=0.03, respectively.

3.1.2 CG30 model

The selection of a child grid domain configuration is sensitive to the location of boundaries that may affect the overall stability and performance of the nested model solution. Suitable CG boundaries must be located in areas of low PG inaccuracy and at a sufficient distance from the area of interest as location of the boundary close to the area of interest may result in boundary errors propagating into the area causing the accuracy of the solution to deteriorate. On the other hand, boundaries need to be sufficiently close to the area of interest in order to minimize the domain size (computational cost).

The first level child grid, CG30, was located in the north-west part of Cork Harbour with the centrally located Lough Mahon (directly feeding to the River Lee estuary) being the area of interest. The boundaries for the CG30 domain were chosen based on the RE_T distribution plot for the PG90 current velocities presented in Fig. 6. The upper section of Passage West, connecting Lough Mahon with Lower Harbour, was selected as a suitable southern boundary (SB) due to its relatively low RE_T while the closest suitable location for the eastern boundary (EB) was at a much greater distance from Lough Mahon due to generally high PG inaccuracies in the North Channel.

The accuracy of the CG30 boundary location was assessed by comparing the net fluxes of mass and momentum across the corresponding interfaces in the PG90, SG30 and CG30 models. Net fluxes were calculated normal to boundaries. Mass and momentum fluxes through the SB and EB boundaries are compared in Fig. 9 and 10, respectively. It can be seen that the predominant forcing-boundary for the CG30 domain is the SB boundary. The tidally-averaged errors in PG90 fluxes relative to the SG30 were approximately 4% for both mass and momentum indicating a high level of PG90 accuracy. At the EB boundary, the PG90 accuracy was slightly lower resulting in error in PG90 mass flux of 5% and momentum flux of 10%. However, this boundary accounted for a smaller portion of the total boundary forcing, and its distant location from the area of interest allowed boundary errors more time to dissipate. The tidally-averaged errors in CG30 fluxes (both mass and momentum) relative to PG90 fluxes were less that 2% at both boundaries, demonstrating high levels of conservation from parent grid to child grid.

Relative error analysis was also carried out for the entire CG30 model domain with respect to water elevations and velocities, and results of these analyses are summarized in Table 2. The domain-averaged relative error (Equation 8) in the PG90 water elevations relative to the SG30 were 5.9% while in the CG30 model this error was reduced to 1.1%. The extent of the domains with RE_T greater than 1% was 94% for PG90 and 28% for CG30. The absolute error (Equation 9) was also calculated. AE_T in water level significantly decreased from 8cm in the PG90 to 1.2 cm in the CG30. In relation to current velocities, the RE_D was reduced from a large value of 22.4% in PG90 to just 0.5% in CG30; while RE_T values exceeding 5% were found in 72% and 4% of the PG90 and CG30 domains, respectively.

As shown in Fig. 7, timeseries of water elevations and current speed show very good agreement between SG30 and CG30 throughout the tidal cycle. This indicates significant improvement in the accuracy of velocity computation using the high resolution nested CG30 and is verified by the linear regression analysis shown in Fig. 8. The superiority of CG30 over PG90 model when compared to SG30 is clear and confirmed by a correlation coefficient of 0.99 compared to 0.89. The slope and intercept were also improved for CG30 when compared to PG90; with m=1.01 and c=-0.01 the CG30 against SG30 model solutions lie approximately on the 45° line.

These results demonstrate that the application of the nested high resolution model results in significant improvement in the accuracy of the model solution over the lower resolution PG solution. Similar to the improvement in model accuracy, an equally significant reduction in computational effort was achieved. For example, the application of MSN_Flood model to level 1 domain nesting yields 21 minutes simulation time for the PG90-CG30 model; this is contrasted by 80 minutes simulation time for the SG30 model. Thus the nested model runs 3.8 times quicker than the single grid model.

3.1.3 CG06 model

In contrast to the CG30 grid being fully embedded within the PG90 grid, in the second level of nesting CG06 is only partially nested within its parent CG30 (Fig. 4). Approximately 38% of wet cells in CG06 overlap CG30. This is a hybrid boundary structure where the east boundary is prescribed using hydrodynamic data from the parent model while the west boundary is prescribed using measured data. The west boundary is a flow boundary, with River Lee inflows extracted from river gauging station 19011. The east boundary is a water elevation boundary where water elevations are supplied along the boundary by the CG30 model. The location of the latter boundary was selected to correspond to the position of the Tivoli tidal gauge station and therefore to contribute to model validation (see Fig. 3 for location of Tivoli gauge).

Validation of the CG06 model is conducted for the flood event of November 2009, which due to a combination of heavy river discharges and high tides coinciding with moderate surges resulted in extensive inundation of the area delineated by this nested grid. Figure 11 compares timeseries of water elevation computed at the CG30-CG06 nested boundary (east boundary) against tidal gauge records from the same location. Overall, there is a very good agreement between predicted water elevations and measured data. The high degree of model accuracy is manifested by high correlation (0.992) and a low value of RMSdiff (0.022m) shown in Table 3 (model CG06_1). Both the RMSE (0.142m) and centred RMSD (0.141m) indicate that the model is able to reproduce variability of water elevation with a good accuracy (order 0.14m). Further, a small difference between these two statistical measures implies that the mean values of observations and simulation are very close. Interestingly, the accuracy of the CG06 model is improved when a 6 minutes phase shift (one record timestep) between observations and simulation is artificially introduced (model CG06_2 in Table 3). This results in RMSE (RMSD) reduction to 0.106m (0.104m) and an increase of correlation to 0.996. It is deemed then that there is a phase lag between model and observations of approximately one observational timestep. Another aspect of the analysis involved temporal occurrence of an error. As the model-observations discrepancies are observed around low water levels (which is not so significant to this study), by not considering negative water elevations (below 0 mOD Malin) the RMSE is further reduced to 0.075m (model CG06_3 in Table 3). Such level of agreement between model and observation is considered to be satisfactory.

The effect of horizontal resolution on model skill is also examined. This is carried out by comparing the model performance at 6 m and 2m resolutions. For this purpose a single grid 2m reference model (SG02) covering the area delineated by the CG06 model was developed. Figure 12 presents the distribution of water level RE_T in the CG06 solution relative to the SG02 reference solution. In general, errors in CG06 outside the Cork City centre are very low (<10%) implying that flooding in the rural area of Cork is well resolved using the 6m grid. In contrast, significantly higher errors are obtained in the Cork City (CG02 domain), and in particularly in areas of narrow dense streets where errors exceed 30%. Here, an increase in model resolution leads to a significant reduction in errors. This implies that next level of nesting is required to improve the model accuracy in the city centre.

3.1.4 CG02 model

Finally, the highest resolution 2m model (CG02), fully embedded within CG06, covers the urban area of Cork City; this area is particularly prone to flooding. In the first step of model skill analysis, water elevations simulated by the CG06 and CG02 models at four locations along the river channel are compared in Fig. 13 and statistically summarized in Table 4. Again, the November 2009 flood event was used as a benchmark. Close to the east boundary, at point CG02_4 (see Fig. 14 for point location), both models perform almost identical and this is visually and statistically confirmed in Fig. 13d and in Table 4, respectively. Discrepancies between the CG06 and CG02 models increase with distance from the nested east boundary and are manifested by overall higher water elevations computed by the coarser CG06 model. Location CG02_2 (Fig. 13b) shows the biggest discrepancy evidenced by the statistical measures RMSE=0.195m, RMSD=0.109m, RMSdiff=-0.181m. Despite overprediction of water elevations by the CG06 model, the general water level trends in the two models are in good agreement (COR=0.997). Another important advantage of a high resolution model is an improved numerical stability of the model solution. As can be seen from Fig. 13 a-c, some infrequent random oscillations in water levels occurring in CG06 from numerical instability due to insufficient grid resolution are not present in the finer CG02 model.

The numerical instability of the MSN_Flood model is directly related to the grid resolution and results from an alternating direction implicit (ADI) algorithm used in the model's solution procedure. In general, the models using ADI are very accurate numerically in modelling flows, however, in the presence of a discontinuity, such as in regions of sharp gradients (e.g. velocity gradients, elevation gradient or high elevations), the numerical models using such schemes are prone to generate spurious numerical oscillations (Kvočka et al., 2015). A common solution used to reduce these oscillations is to increase the grid resolution so the slopes over numerical grids are milder. Comparing time series outputs from CG06 and CG02 (Fig. 13), it is evident that increasing resolution of the model significantly reduces numerical errors and hence oscillations.

The effect of improved horizontal resolution is analysed spatially by means of RE_T distribution plots. As shown in Fig. 12, the 2m resolution is essential to resolve small scale processes of complex urban area. Figure 14 compares RE_T between CG02 and SG02. In general, RE_T is quite low at 10% in the western part of the city along river banks increasing in eastward direction to 20% in narrow streets of city centre. This is a considerable improvement when compared to RE_T in CG06 relative to SG02. Moreover, as CG02 achieves a similar level of accuracy to SG02 the computational cost is significantly reduced and constitutes enormous 96% saving.

From this analysis it can be seen that the CG06-CG02 nesting results in a model performance generally comparable to the single grid SG02 model but at a significantly reduced computational cost when compared to the single grid model.

The ultimate conclusion from the model validation is that MSN_Flood facilitates significant improvements in model accuracy without incurring the computational expense of high spatial resolution over the entire model domain. The model setup constitutes a rigorous test of model performance and on that basis it can be further concluded that the model is applicable to situations where nested boundaries are located in complex urban floodplains that periodically wet and dry.

3.2 Urban flood modelling

For most of the time, city streets are dry and rivers draining the hinterland are contained within well-defined river banks or walls. However, when extreme flood events occur rivers may burst their banks and the city streets become water conveyance channels. The simulation of the hydrodynamics associated with rapid urban flood events is complex; many significant issues must be addressed such as flooding and drying, spatial resolution, domain definition, frictional resistance and boundary descriptions. When modelling flood events, the mathematical formulation of the nested boundaries that permit flooding and drying is of particular importance. Also, the horizontal resolution necessary to resolve small scale processes must be considered. In particular, these aspects of the MSN_Flood model will be discussed in this section.

3.2.1 Extreme flood event

On the 19th and 20th of November 2009 high River Lee flows combined with high astronomical tides and moderate surge caused localized overtopping/breaching of the river banks resulting in widespread flooding of Cork City. Evolution of the flood wave propagation simulated by the CG02 model is shown in Fig. 15. Maximum flooding was reached at 9:30 on 20/11/2009 around the time of high tide and approximately 5 hours after peak discharge of River Lee. At this juncture over 62ha of Cork City had been flooded. The most affected zone was the city centre located between the north and south channels of the river; this area is a low-lying island that over centuries was gradually reclaimed from marshland and it's low-lying topography combined with the influence of river, estuary and harbour makes the area particularly vulnerable to flooding.

The accuracy of the urban inundation simulation was assessed against field observations of inundation extent and maximum heights of flood waters. The observed and modelled ultimate extents of flooding in the city are shown in the Fig. 16; the hindcasted extent of inundation matches very well that observed during the flood event. With regards to flood level heights, observed water level marks were collected and post-processed by OPW at 38 survey points across the flooded area; their distribution is shown in Fig. 17. The survey point data were subsequently used to calibrate the model. Initial calibration tests showed that the model was most sensitive to bottom roughness coefficient. An extensive statistical analysis of bed roughness parameterization was used to provide an accurate model solution for flood inundation. The best fitting results (R=0.97, RMSD=0.26) were obtained for the following roughness values: upper channel=0.90, lower channel=0.90, roads=0.1, city floodplain=0.1 and upstream floodplain=0.30. Figure 18 provides visual assessment of the best fit model skill; good agreement between the model and observations is achieved as the model solution falls on the 45° line. Interestingly, better agreement was found for survey locations in floodplains as opposed to points adjacent to the river bank. This could be attributed to the fact that the majority of survey points are located away from the channel edge (many are actually at the floodplain edge).

3.3 Moving boundary

The specification of a nested boundary in a flood-prone area is particularly problematic; nested models developed so far prohibit flooding and drying along open boundaries. This problem has been overcome in MSN_Flood; its unique mathematical formulation of the nested boundary involving ghost cells, internal boundary formulation and adaptive interpolation, ensures stable flooding and drying of boundary cells. In MSN_Flood, any nested boundary can be placed within a flooding and drying zone and therefore may be subject to significant lateral expansion and contraction. Moreover, the internalization of the boundary allows the flooding and drying mechanism to approach the boundary of the nested domain from either upstream or downstream. As the boundary alternatively floods or dries, the number of active boundary cells expands and contracts accordingly. Depending on local topography, not only the length of the boundary may change but also the number of active boundaries changes. Such a boundary is therefore a complex, non-continuous, moving boundary that spatially and temporally changes its characteristics. This is a significant aspect of this research.

In the model setup, the urban CG02 model is entirely embedded within the CG06 model; mass and momentum from the 6m model is transferred to the 2 m model via two nested boundaries – the western boundary transferring River Lee waters from the upper to the lower channel of the river (it also geographically divides the floodplains into upper and lower floodplains), and the eastern boundary exchanging waters with the estuary. The western boundary of CG02 is located on the upstream fluvial floodplain which is prone to wetting and drying. A cross section through this boundary illustrating the steep gradients of the river channel bathymetry and the topography of the adjacent urban floodplains (which includes buildings) is shown in Fig. 19. The temporal progression of water levels throughout the November 2009 flooding is also plotted. The reference water level at simulation time t=4hr corresponds to a 187 m^3/s river flow (19th of November 2009 at 01:30). At this juncture the flow greatly exceeds the average river flow of 40 m^3/s as it results from increased discharges from Inniscarra dam. The storage capacity of Inniscarra Reservoir had been reached after a month-long period of record high rainfalls and heavy downpours on the 18th and 19th of November. Over the course of the subsequent 28 hours the discharges further increased to reach a maximum value of 560 m^3/s at 2:30 on November 20th. The water level at the boundary increased from 4.57 mOD at 22:30 November 18th to a peak of 5.74 mOD 28 hours later.

The extensive inundation of the upper channel floodplains (upstream floodplains) has a major effect on the western boundary of the CG02 model. It can be seen in Fig. 19 that as the flooding progresses to a simulation time of 8hrs a second wetted boundary is created south of the main channel boundary due to bifurcation of flood waters into two channels (called here the main and side channels) approximately 1.2km upstream of the boundary. Importantly, there is a significant difference in water elevation of 0.41m between the two channels of the boundary. This results from the topography of the upstream floodplains and therefore local flow conditions. The reason for the difference in water elevations along the two sections of the boundary can be explained with the help of Fig. 20 showing three cross-sections including one (cross-section 3) located close to the nested western boundary. As simulated by the CG06 model, downstream from cross-section 1, representing the maximum cross-sectional extent of the inundated area, flood waters must flow around an elevated strip of rural land and so splits at this point into two floodplain channels. This is shown in cross-section 2, located at mid length of this 1 km long strip of land; here the water elevation difference between two channels is 0.31m. This elevation difference further increases to 0.41m near the nested boundary (cross-section 3).

The temporal rise of water levels at a number of points across the western nested boundary is shown in Fig. 21. Series A represents the main river channel, series B and C correspond to points adjacent to the river channel while series D is located in the side channel. The difference in water elevations between the two boundaries is apparent throughout the entire flooding period, though it is reduced with the progress of flooding.

An interesting characteristics of the moving boundary is it change in its length. As flood waters continue overtopping the river banks, the area of inundation increases and is reflected in the elongation of the boundary. The length of the main channel boundary is initially equal to the river width, this nearly doubles during flooding as shown for t=12 hrs in Fig. 19. The temporal evolution of flooding through the boundary clearly demonstrates that the nested boundary is a discontinuous moving boundary with a variable head.

The numerical stability of such dynamically changing properties of nested boundary is an important aspect of nesting procedures. Overall, a change in length as well as division into separate subsections does not markedly impact computational stability nor model performance. In fact, as shown in Fig. 14, RE_T computed over the flooding period remain low within the CG02 domain despite significant changes to nested boundary configurations and flow conditions.

As demonstrated in this section MSN_Flood is developed in a general-purpose manner that through stable and accurate moving boundary provides a high degree of choice and flexibility regarding the location of the boundaries to the nested domain.

3.4 Model resolution

Due to the highly irregular topography of urban environments and the highly dynamic flows involved, urban flooding is a complex problem. Most of the flood models developed so far have focused on rural or semi developed floodplains where isolated large structures can be modelled while small objects are ignored or parameterized as bottom friction (Brown et al., 2007). Such modelling does not implicitly account for locking effects of building on flow. As the presence of buildings may substantially increase flood extent when compared with undeveloped floodplains the role of high resolution discretization is paramount. However, as Brown et al., (2007) found, the greatest source of modelling error with respect to grid resolution is associated with the steepest gradients in topography which are susceptible to interpolation error.

Modelling of flood flow through urban area is difficult because of its need for stable and accurate solution of the flow equation (Brown et al., 2007**)**. Since accurate modelling requires a resolution commensurate with flow features, dense street network flows through urban floodplains can only be fully resolved with a sufficiently high resolution. However, satisfactory model resolution, and thus accuracy, incurs computational expense; a balance between these two contradicting factors provides an optimal solution. Gallegos et al. (2009) found that a 5m resolution mesh that spans a street by approximately three cells achieves such balance. The characteristics of urban residential areas of southern Californian investigated in their study is different than that of an old European development type towns comprising of narrow dense streets as Cork City. It follows that the 5m model resolution is insufficient to resolve flow dynamics in such city centre street networks.

In order to analyse the overall effect of model resolution on simulation results, CG06 and CG02 model results are compared. Visual comparison of flood inundation can be made from Fig. 22 which shows CG06 and CG02 model outputs representing the maximum extent of inundation during the November 2009 flooding. There is a discrepancy in the extent and magnitude of flooding between the two models. Some zones and streets do not get flooded in the CG06 model, which may be caused by the coarse representation of the street network and associated lack of connectivity between certain streets, while in other zones flood water is present in areas which remain dry according to observations and CG02 output. Figure 23 (a) shows the difference in water elevations between CG02 and CG06 interpolated onto the 2m grid. It is clear that both the height and area of flooding are affected. The absolute difference in water level is on average 0.13m and is underestimated by the 6m model by up to 0.4m in the upper section of river and overestimated by approximately 0.3m in the lower section. Figure 23 (b) shows a spatial distribution of RMSE between two models. There is a noticeable reduction in model performance at coarser resolution of 0.08m RMSE over the entire domain and the error is generally larger in the dense street network of the urbanized zone. Based on model results it is clear that a substantial portion of the error results from the coarse representation of topography since its gradient is greater that the slope in water surface; however, some small portion of the error could be attributed to errors in LIDAR data (~0.1m RMSE according to Bates et al, 2010) as well as interpolation from 6m down to 2m grid.

Another comparative measure involves a computation of relative differences (Equation 10) in inundated area and flood water volume between fine and coarse grid models at a particular time. Figures 24 (a) and (b) show the evolution of differences between CG02 and CG06 solutions in inundated areas and volumes throughout the simulation. The significantly high relative difference in the area at the initial stage of flooding reaching 36% is misleading as the relatively small total inundated area with a small flood time lag results in large discrepancies at this stage (ca. 11ha). Nevertheless, when the flooding is more pronounced (over 30 ha, max 62.6ha) the relative difference is still up to 10%. With regards to flood water volume in inundated areas the difference is over 20% during first hours of flooding and still remains as high as 10% throughout the flood peak only falling to below 10% when the flood recedes. The total RMSE of inundated area and volume between 2m and 6m models are 3.4ha and 21,367m^3. This comparison demonstrates that horizontal resolution is of paramount importance when simulating flows through complex topography. It seems that for Cork City centre comprising of dense network of narrow streets, neither the 5m resolution requirement nor 3 cell street span would resolve complex flood flow at satisfactory level of accuracy.

3.5 Flood water velocities

Another significant advantage of MSN_Flood is its ability to simulate the velocities of flood waters. As opposed to simplified 2D hydraulic models frequently used in urban flooding, the hydrodynamic MSN_Flood includes both the continuity and momentum equations, solving for both water elevations and water velocities. Figure 25 shows an example of flood water velocities computed by MSN_Flood in a selected area of Cork city centre blown up for ease of viewing; one can see flood waters in both the river channel and the urban floodplain. This zone is characterized by fast flowing shallow water subject to rapid transitions as it flows down through the steep section of recreational grounds adjacent to the river channel. The city downtown, in contrast, is a ponding area with relatively stagnant waters.

Knowledge of velocity fields facilitates better understanding of flood water hydrodynamics and in particular the mechanisms of flood propagation. The routes and speeds of flood waves provide important information for the evaluation of flood risks to people's safety and to property, as well as to the planning and actions of emergency response teams.

4 Discussion

Inundation of coastal areas due to coastal and/or fluvial urban flooding mechanisms is a very complex hydrological phenomena, and developing a modelling system to accurately simulate it is not a trivial task. The research presented in this paper demonstrates that the concept of nesting models is very suitable for complex urban coastal flooding as they facilitate the development of an integrated system capable of resolving hydrodynamics at spatial scales commensurate with flows and physical features of the region of interest. The modelling system adopted here determines physical processes simultaneously at different scales ranging from bay-size circulation (90 m) through mesoscale processes of coastal waters at 30 m resolution down to the ultra-high scale environment of 2m. Validation results show that the model performs well at each of these scales.

The MSN_Flood model developed for use in this research is well suited for high resolution urban flood simulation for a number of reasons. Firstly, it allows smooth transition of the model solution between coastal waters and river floodplains while giving a very high level of conservation of mass and momentum between parent and child grid (Nash and Hartnett, 2010). Through incorporation of ghost cells and formulation of a dynamic internal boundary, MSN_Flood is designed to minimize boundary formulation error and therefore to transfer mass and momentum across the nested boundary without loss of nested solution accuracy. The reduction in boundary errors yields also a significant improvement in model stability at the nested boundary and CG accuracy. This in turn permits stable flooding and drying at the boundary; moreover, these process are allowed to approach the boundary of the nested domain from either upstream or downstream. The so-called moving boundary allows then embedding of a child grid model within the parent model in areas where the nested boundary may wet or dry making the model highly flexible in application. Interestingly, such highly reduced boundary formulation errors is achieved in a nesting mechanism where the nested boundary comprises of only two cells of columns or rows (ghost cells and internal boundary cells). For comparison, in many nested models poor accuracy due to boundary formulation errors is commonly compensated by indirect solutions such as boundary configuration (e.g. location). For example, Kashefipour et al. (2002) in order to reduce possible nesting error dynamically link 2D coastal model with 1D river model by using overlapping grids at the boundary – a common area where boundary values are exchanged between two models. Such model setup is not required in MSN_Flood where accurate exchange of boundary conditions occurs along a boundary.

Secondly, the model has virtually no limit to the number of specified nesting levels (and spatial resolution) and is primarily constrained by computational effort rather than numerical stability. The highest resolution of 2 m set for this study was dictated solely by the resolution of available LiDAR data and higher resolutions are easily achievable if suitable terrain data is available. For example, a 0.025 m resolution was used to simulate flows corresponding to those in a physical scale model of a harbour of dimensions 1.0x1.0x0.25 m (Nash and Hartnett 2014). In this way, the model allows improved accuracy of solution when compared to a lower resolution parent model where the improved accuracy is similar to that of a similar high resolution single grid model but the computational effort is significantly reduced.

Thirdly, the model provides adequate solutions at scales sufficient for processes of interest, such as coarse resolution coastal circulation and fine resolution flood inundation. This is attributed to the robust hydrodynamic module which in essence adopts the well-tested numerical scheme and discretisation methods described by Falconer and Chen (1991). The uniqueness and improvement of MSN_Flood over other nested models is its formulation of the nested boundary in the area where flooding and drying may occur. In order to accommodate flooding and drying of boundary cells the model allows a moving nested boundary so that large sections of the boundary can alternatively wet and dry. The stable flooding and drying of boundary cells results from the internalisation of the nested boundary combined with an adaptive interpolation technique tailored specifically for this model. To the author's knowledge the development of a non-continuous moving nested boundary in a circulation model is novel. Such an innovative solution does not pose restrictions on the location of nested grids with regards wetting and drying (as demonstrated by the application to Cork Harbour) and, therefore, allows flexibility of model setup.

Finally, in the context of urban flood modelling, MSN_Flood's ability to simulate horizontal components of water velocity is a significant advantage over simpler hydraulic models commonly used in flood modelling; the complexity of urban topography (buildings, vegetation, walls, roads, embankments, ditches etc) necessitates at least two-dimensional treatment of surface flows (Cook and Merwade, 2009). Spatial and temporal distribution of velocity fields is also required for assessment of flood risk to people and property associated with a certain flood flow magnitude. Thus, this feature will greatly benefit flood hazard management.

Although the modelling framework seems to be the main factor controlling accuracy of model predictions, other factors such as model resolution, datasets and model parameterization also play a crucial role. In relation to model topography/bathymetry, these aspects are interconnected and need to be considered jointly. Comparing the 6m and 2 m grid models it can be seen that results are quite sensitive to the spatial resolution of the model. The resolution acts as a filter on the model terrain so the model error increases with decreasing spatial resolution, as the definition of topographic features (walls, hedges etc) are progressively lost from the model bathymetry. There is a dual effect of this. Firstly, as the resolution becomes less granular the topographic complexity of high density small features become sub-grid phenomena which then become parameterised through roughness coefficients. Spatially varying roughness needs to be specified for different terrains, this is determined based on surface classification (such as land type, vegetation or roads) within model sensitivity and calibration. Secondly, the loss of larger objects such as buildings makes the model inherently ill-conditioned and their loss cannot be remedied through modification of roughness coefficient alone. Errors are additionally amplified by a presence of bias in the topographic data resulting from LIDAR related post-processing difficulties such as representation of surface objects discussed in Mason et al. (2003).

5 Conclusions

In this research, high-resolution multi-scale modelling of coastal flooding due to tides, storm surges and rivers inflows is performed. The MSN_Flood modelling system is used to simulate flood water inundation of Cork City. The main findings from this research fall into two categories as follows:

1. Model computational performance:

   (a) The nesting model framework allows the model operation at practically any desired horizontal resolution, including scales commensurate with resolution of LiDAR data making an optimal use of such datasets. In the current setup, a four-nest cascade telescopes resolution down to the level of LiDAR resolution which is sufficient to capture small scale flow features.

   (b) The model has no limits as to the number of nesting levels and the numerical stability is maintained down to the finest resolution.

   (c) Computational effort is dictated by the number of nesting levels, the horizontal resolution of each nested grid and the extents of each nested grid. Nevertheless, at the finest resolution the nested model was found to be almost as accurate as a single grid model of the same resolution but at 96% saving in computational cost.

   (d) Due to its robust flooding and drying routine, the model maintains numerical stability and accuracy in any part of the model domain affected by these processes.

   (e) Internalisation of the nested boundary through a use of ghost cells combined with a tailored adaptive interpolation technique permits flooding and drying of the nested boundary creating highly dynamic moving boundaries. Moreover, the flooding and drying mechanism can approach the boundary of the nested domain from either upstream or downstream. Nesting with a moving boundary allows embedding of a child grid model within the parent model in areas where the nested boundary may wet or dry. This unique feature of MSN_Flood provides a high degree of choice regarding the location of the boundaries to the nested domain and therefore flexibility in model application. This capability gives MSN_Flood significant advantages over other models.

2. Model accuracy:

   (f) The modelling system demonstrates a good capability to accurately determine physical processes at different spatial scales including mesoscale coastal water circulation (90m) and small scale hydrodynamics of complex urban floodplains (2m).

(g) The extent of flood inundation into floodplains of Cork City and maximum water levels reached during flooding were accurately simulated by the urban flood 2 m grid model.

(h) Fine horizontal resolution is crucial for accurate assessment of inundation. Comparison of 6m and 2m grid model RE_T in water levels shows a noticeable reduction in model performance at coarser resolution over the entire domain and the error is generally greater in the dense street network of urbanized zone.

(i) The urban flood model provides full characteristics of water levels and flow regimes necessary for assessment of flood risk to people's safety associated with particular flood water levels and associated flood water velocities.

To conclude, near-unlimited model resolution, geographically unconstrained (due to wetting and drying) nested model setup, robust wetting and drying routine, computational efficiency and the capability to simulate both water elevations and velocity fields, make the MSN_Flood a valuable tool for studying coastal flood inundation. This research demonstrates that the adopted methodology can be successfully used in applications to coastal flood modelling including complex urban environments. It can provide, at specific instances of time, accurate spatial distributions of water elevations and flow magnitudes in inundated areas and can, thus, provide critical information to assess possible extents of flood inundation, periods of inundation, maximum water elevations reached and flood wave propagation routes and speeds. Ultimately, it can be directly used for evaluation of flood risks to the area and indirectly, through some functional relationships, for risk assessment of human safety and property damage. The methodology explored in this research, when applied in a forecasting sense, constitutes a high resolution flood warning and planning system that can aid local decision makers targeting high flood risk areas.

Acknowledgements

This publication has emanated from research conducted with the financial support of Science Foundation Ireland (SFI) under Grant Numbers SFI/12/RC/2302 and SFI/14/ADV/RC3021.

References

Bates, P.D., Dawson, R.J., Hall, J.W., Horritt, M.S., Nicholls, R.J., Wicks, J., Hassan, M.A.A.M.: Simplified two-dimensional numerical modelling of coastal flooding and example applications. Coastal Engineering 52, 795-810, 2005.

Bates, P.D., De Roo, A.P.J.: A simple raster-based model for flood inundation simulation. Journal of Hydrology 236, 54-77, 2000.

Bates, P.D., Horritt, M.S., Fewtrell, T.J.: A simple inertia formulation of the shallow water equations for efficient two-dimensional flood inundation modelling. Journal of Hydrology 387, 33-45, 2010.

Brown, J.D., Spencer, T., Moeller, I.: Modeling storm surge flooding of an urban areas with particular reference to modelling uncertainties; A case study of Canvey Island, United Kingdom. Water Resources research 43, W06402, 2007.

Chen, X.: Dynamic coupling of a three-dimensional hydrodynamic mode with a latterly averaged, two-dimensional hydrodynamic model. Journal of Geophysical Research 112, C07022, 2007.

Cook, A., Merwade, V.: Effect of topographic data, geometric configuration and modelling approach on flood inundation mapping. Journal of Hydrology 377, 131-142, 2009.

DHI Software, 2001. Mike 21 flow model: hydrodynamic module user guide. DHI water and Environment.

Falconer, R.A.: A mathematical model study of the flushing characteristics of a shallow tidal bay. Proc Inst Civil Eng 2 Res and Theory 77, 311-332, 1984.

Falconer, R.A., Chen, Y.P.: An improved representation of flooding and drying and wind stress effects in a 2-D tidal numerical model. Proc Inst Civil Eng 2 res and Theory 91, 659-678, 1991.

Fewtreel, T.J., Duncan, A., Sampson, C.C., Neal, J.C., Bates, P.D.: Benchmarking urban flood models of varying complexity and scale using high resolution terrestrial LiDAR data. Physics and Chemistry of the Earth 36, 281-291, 2011.

Formaggia, L., Gerbeau, J.F., Nobile, F., Quarteroni A.: On the coupling of 3D and 1D Navier-Stokes equations for flow problems in compliant vessels. Comput Methods Appl Mech Eng 191, 561-582, 2001.

Gallegos, H.A., Schubert, J.E., Sanders, B.F.: Two-dimensional high-resolution modelling of urban dam-break flooding: A case study of Baldwin Hill, California. Advances in Water Resources 32, 1323-1335, 2009.

Gomes-Pereira, L.M., Wicherson, R.J.: Suitability of laser data for deriving geographical data: a case study in the context of management of fluvial zones. Photogrammetry and Remote Sensing 54, 105-114, 1999.

Haidvogel, D.B., H. Arango, W.P. Budgell, B.D. Cornuelle, E. Curchitser, E. Di Lorenzo, K. Fennel, W.R. Geyer, A.J. Hermann, L. Lanerolle, J. Levin, J.C. McWilliams, A.J. Miller, A.M. Moore, T.M. Powell, A.F. Shchepetkin, C.R. Sherwood, R.P. Signell, J.C. Warner, J. Wilkin: Ocean forecasting in terrain-following coordinates: Formulation and skill assessment of the Regional Ocean Modeling System. J. Comp. Phys. 227(7), 3595-3624, 2008.

Halcrow: Lee catchment flood risk assessment and management study. Hydrology report. Halcrow Group Ireland Ltd. , 2008.

Holt, J., Harle, K, Proctor, R., Michel, S., Ashworth, M., Batstone, C., Allem, I., Holems, R., Smyth T., Haines, K., Bretherton, D., Smith G.: Modelling the global coastal ocean. Philos Trans Soc A 367, 939-951, 2009.

Horritt, M.S.: Calibration and validation of a 2-dimensional finite element flood flow model using satellite radar imaginary. Water Resources Research 36, 3279-3291, 2000.

Horritt, M.S., Bates, P.D., Mattinson, M.J.: Effects of mesh resolution and topographic representation in 2D finite volume models of shallow water fluvial flow. Journal of Hydrology 329, 306-314, 2006.

Hunter, N.M., Bates, P.D., Neelz, S., Pender, G., Villanueva, I., Wright, N.G., Liang, D., Falconer, R.A., Lin, B., Waller, S., Crossley, A.J., Mason, D.C.: Benchmarking 2D hydraulic models for urban flooding. Water Management 161, 13-30, 2008.

Kashefipour, S.M., Lin, B., Harris, E., Falconer, R.A.: Hydro-environmental modelling for bathing water compliance of an estuarine basin. Water Research 36, 1854-1868, 2002.

Korres, G., Lascaratos, A.: A one-way nested eddy resolving model of the Aegean and Levantine Basins: implementation and climatological runs. Ann Geophys 21, 205-220, 2003.

Kvočka, D., Falconer, R.A., Bray, M. : Appropriate model use for predicting elevations and inundation extent for extreme flood events. Natural Hazards 79, 1791-1808, 2015.

Lin, B., Falconer, R.A.: Tidal flow and transport modelling using ULTIMATE QUICKEST scheme. Journal of hydraulic Engineering 123, 303-314, 1997

McMillian, H.K., Brasington, J.: Reduced complexity strategies for modelling urban floodplan inundation. Geomorphology 90, 226-243, 2007.

Mark, O., Weesakul, S., Apirumanekul, C., Aroonnet S.B., Djordjevic, S.: Potentials and limitations of 1D modelling of urban flooding. Journal of Hydrology 299, 284-299, 2004.

Marks, K., Bates, P.D.: Integration of high-resolution topographic data with floodplain flow models. Hydrological processes 14, 2109-2122, 2000.

Mason, D.C., Cobby, D.M., Horritt, M.S., Bates, P.D.: Floodplain friction parameterization in two-dimensional river flood models using vegetation heights derived from airborne scanning altimetry. |Hydrological Processes 17, 1711-1732, 2003.

Mason, D.C., Horrit, M.S., Hunter, N.M., Bates, P.D.: Use of fused airborne scanning laser altimetry and digital map data for urban flood modelling. Hydrological Process 21, 1436-1447, 2007.

Nash, S.: Development of an adaptive mesh inter-tidal circulation model. PhD Thesis Collage of Engineering and Informatics, National University of Ireland, Galway, 2010.

Nash, S., Hartnett, M.: nested circulation modelling of inter-tidal zones: details of nesting approach incorporating moving boundary. Ocean Dynamics 60, 1479-1495, 2010.

Nash, S, Hartnett, M..: Development of a nested circulation model: boundary error reduction. Environmental Modelling and Software 53, 65-80, 2014.

Nittis, K., Perivoliotis, L., Korrea G., Tziavos, C., Thanos, I.: Operational monitoring and forecasting for marine environmental applications in the Aegean sea. Environ Modell Softw 21, 243-257, 2006.

Olbert A.I., Hartnett M.: Storms and surges in Irish coastal waters. Ocean Modelling 34, 50–62, 2010.

Pappenberger, F., Beven, K., Horritt, M., Blazkova, S.: Uncertainty in the calibration of effective roughness parameters in HEC-RAS using inundation and downstream level observations. Journal of Hydrology 302, 46-69, 2005.

Pender, G., Neelz, S.: Benchmarking of 2D hydraulic modelling packages. SC080035/R2 Environmental Agency, Bristol, p. 169, 2010.

Ponte, R.M.: Understanding the relation between wind- and pressure-driven sea level variability. Journal of Geophysical Research 99, 8033-8039, 1994.

Robins, P.E., Davies, A.G., Jones, R.:Application of coastal model to simulate present and future inundation and aid coastal management. J Coast Conserv 15, 1-14, 2011.

Sanders, B.F., Schubert, J.E., Detwiler, R.L.: ParBreZo: A parallel, unstructured grid, Godunov-type, Shallow water code for high-resolution flood inundation modelling at the regional scale. Advances in Water Resources 33, 1456-1467, 2010.

Simmons A.J., Burridge D.M., Jarraud M., Girard C., Wergen W.: The ECMWF medium-range prediction models development of the numerical formulations and the impact of increased resolution. Meteorol Atmos Phys 40, 28-6, 1989.

Smith, L.C.: Emerging applications of interferometric synthetic aperture radar (INSAR) in geomorphology and hydrology. Annals Assoc Am Geography 92, 385-398, 2002.

Uppala, S.M., Kallberg, P.M., Simmons, A.J., Andrae, U., Bechtold, V., Fiorino, M., Gibson, J., Haseler, J., Hernandez, A., Kelly, G., Li X., Onogi, K., Saarinen, S., Sokka, N., Allan, R., Andersson, E., Arpe, K., Balmaseda, M., Beljaars, A., Berg, L., Bidlot, J., Bormann, N., Caires, S., Dethof, A., Dragosavac, M., Fisher, M., Fuentes, M., Hagemann, S., Holm, E., Hoskins, B., Isaksen, L., Janssen, P., McNally, A., Mahfouf, J., Jenne, R., Morcrette, J., Rayner, N., Saunders, R., Simon, P., Sterl, A., Trenberth, K., Untch, A., Vasiljevic ,D., Viterbo, P., Woollen, J.: The ERA-40 reanalysis. Quart J Roy Meteorol Soc 131, 2961-3012, 2005.

Yang, Z., Wang, T., Khangaonkar, T., Breithaupt, S.: Integrated modelling of flood flows and tidal hydrodynamics over coastal floodplains. Environmental Fluid Mechanics 12, 63-80, 2012.

Yu, D., Lane, S.N.: Urban fluvial flood modelling using two-dimensional diffusion-wave treatment: 1. Mesh resolution effects. Hydrological Processes 20, 1541-1565, 2006.

Tables

Table 1. Configuration of nested models

Model	Grid size m	Timestep s	Parent model	Parent-to-model grid ratio
Parent grid (PG90)	90	18	--	1:1
Single grid (SG30)	30	6	PG90	1:1
Child grid 1 (CG30)	30	6	PG90	3:1
Child grid 2 (CG06)	6	0.6	CG30	5:1
Child grid 3 (CG02)	2	0.2	CG06	3:1
Single grid (SG02)	2	0.2	CG06	1:1

Table 2. Summary of error analyses for PG90 and CG30 models within CG30 model area.

Error Analyses Parameter	**SG30**	
	PG90	**CG30**
Water Elevation:		
- RE_D [%]	5.9	1.1
- AE_D [x10^{-2} m]	8.0	1.2
- $RE_T > 1\%$ [%]	94	28
Current Velocity:		
- RE_D [%]	22.4	0.5
- AE_D [x10^{-3} m/s]	2.70	0.13
- $RE_T > 5\%$ [%]	72	4

Table 3. Error statistics of water elevations simulated by the CG06 model and measured at Tivoli tidal gauge station. Heights are in meters

Code	COR	NSD	RMSD	RMSE	RMSdiff
CG06_1	0.992	1.021	0.141	0.142	0.022
CG06_2	0.996	1.023	0.104	0.106	0.024
CG06_3	0.995	1.084	0.075	0.075	0.020

Table 4. Error statistics of water elevations at four locations simulated by the CG06 and CG02 models. Heights are in meters

Code	COR	NSD	RMSD	RMSE	RMSdiff
CG02_1	0.995	1.033	0.080	0.111	-0.081
CG02_2	0.997	1.014	0.109	0.195	-0.181
CG02_3	0.998	1.045	0.056	0.076	-0.064
CG02_4	0.999	0.999	0.006	0.006	0.000

Figures

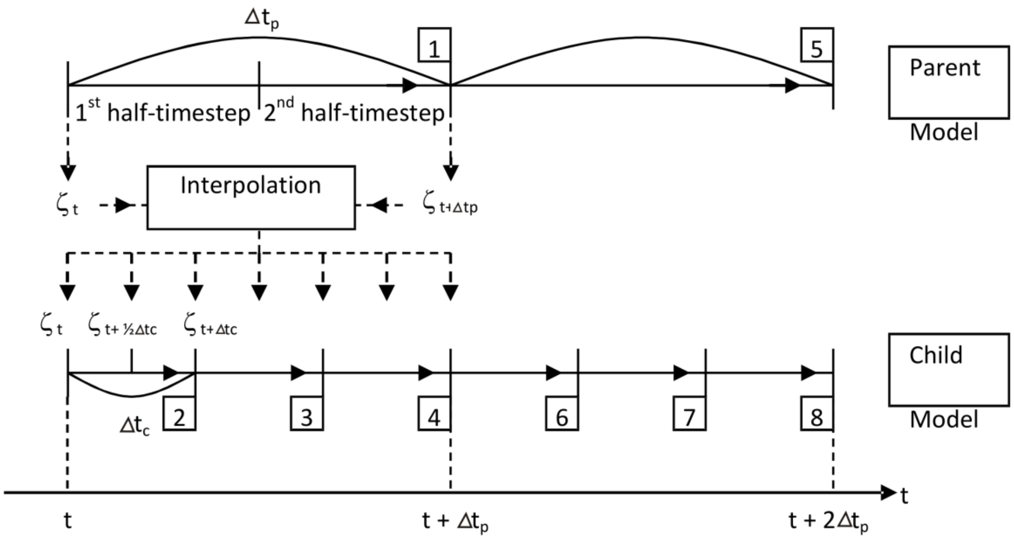

Figure 1: The nesting procedure for a single level of nesting and one variable only - water surface elevation, ζ .

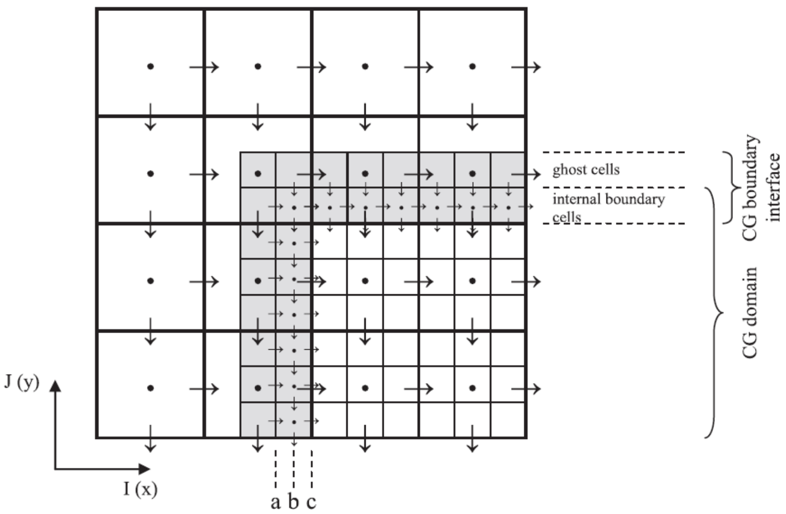

Figure 2: Schematic illustration of the internal boundary configuration for 3:1 nesting ratio.

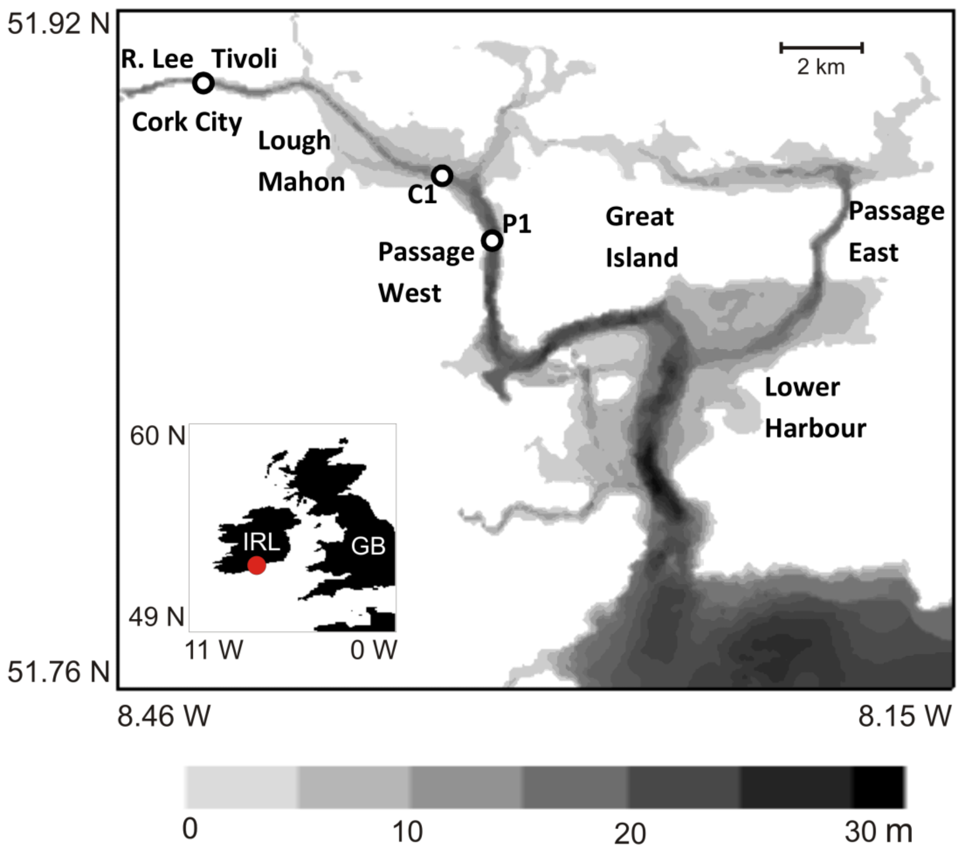

Figure 3: Bathymetry of Cork Harbour (m) with selected locations. Red dot denotes location of Cork Harbour on the coast of Ireland.

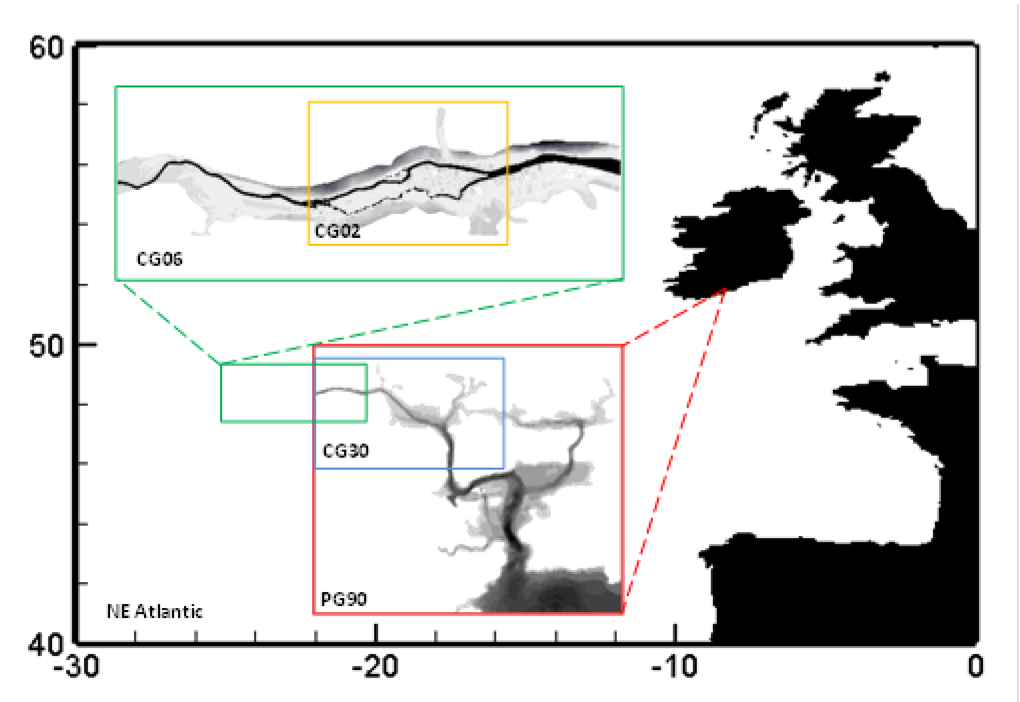

Figure 4: Four-level nesting structure of Cork Harbour and Cork City nested models.

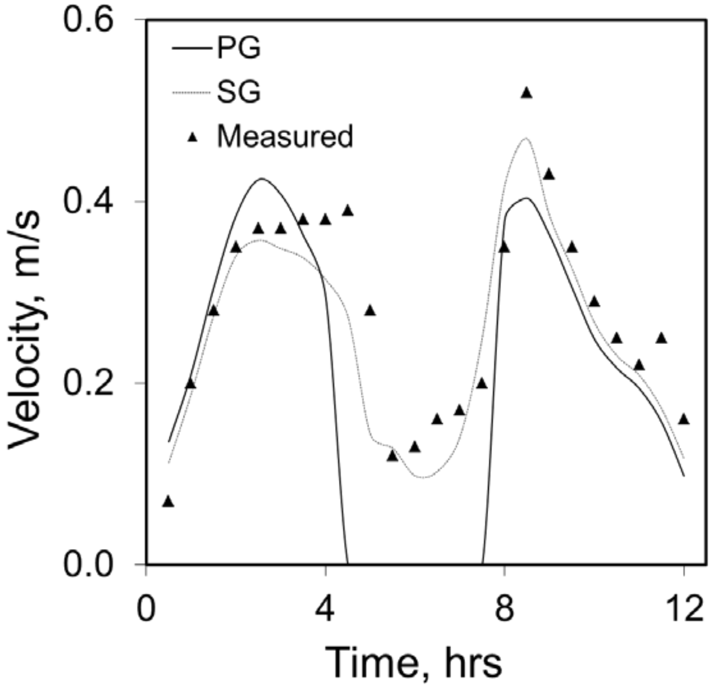

Figure 5: Comparison of computed and measured velocities at point P1in Passage West. Point location shown in Fig. 3.

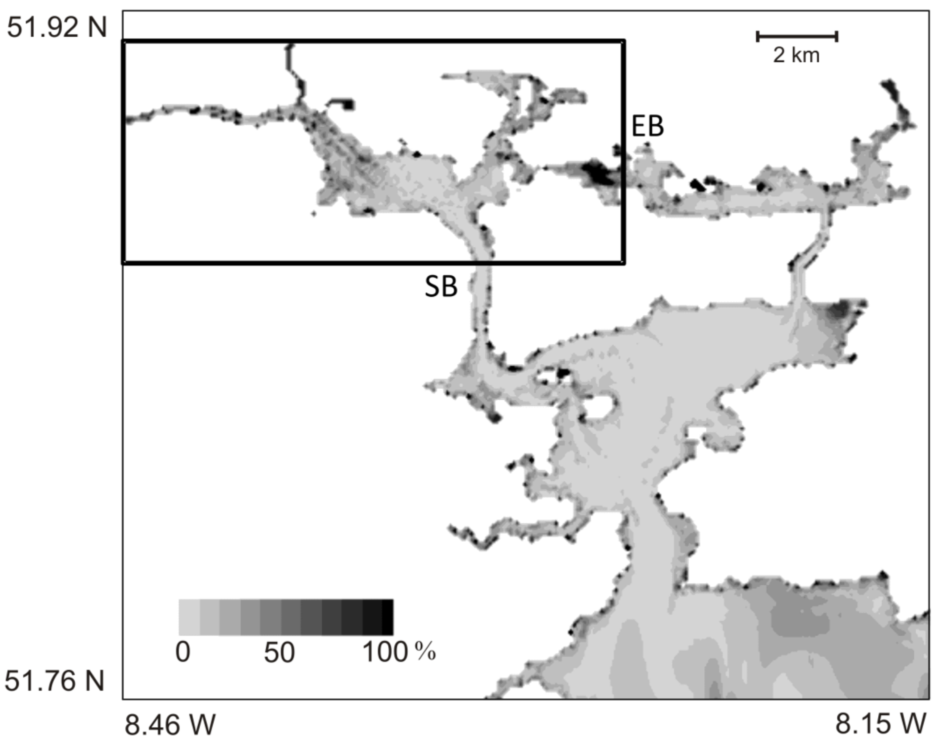

Figure 6: Current velocity RE_T (%) in PG90 relative to SG30. Black box shows the extent of CG30 and locations of nested boundaries. EB - east boundary, SB – south boundary.

(b)

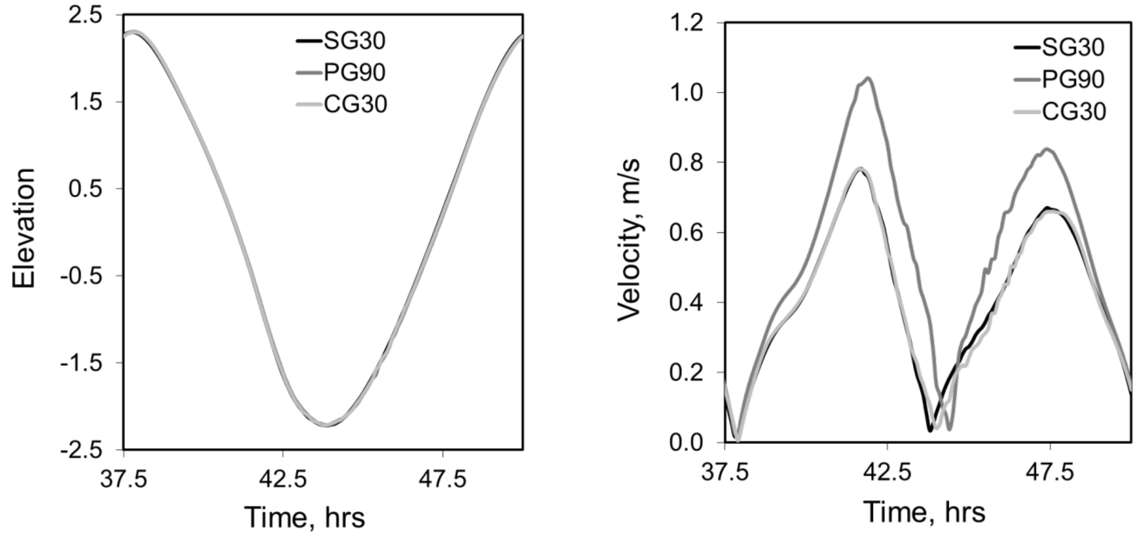

Figure7: Comparison of (a) water elevations and (b) current velocities at point C1 in Lough Mahon. Point location shown in Fig. 3.

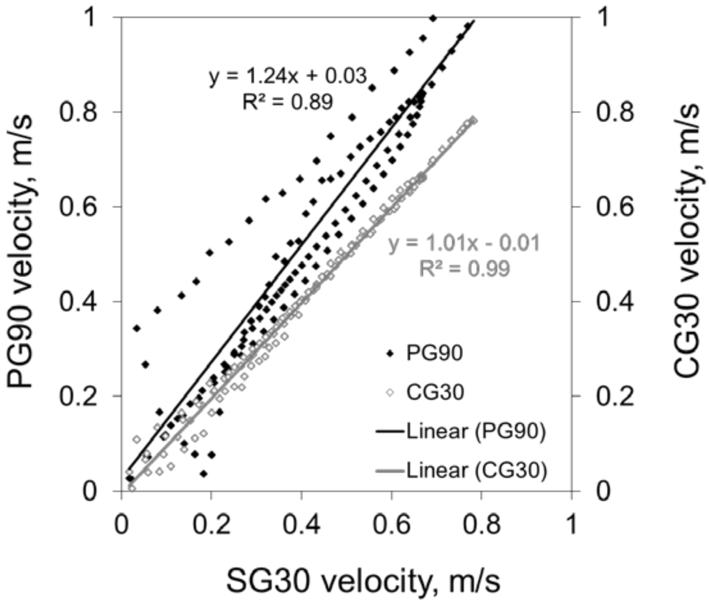

Figure 8: Comparison of modelled velocities for various grid setups at point C1 in Lough Mahon (point location shown in Fig. 3). Time series data are overlain by a linear trend.

(a) (b)

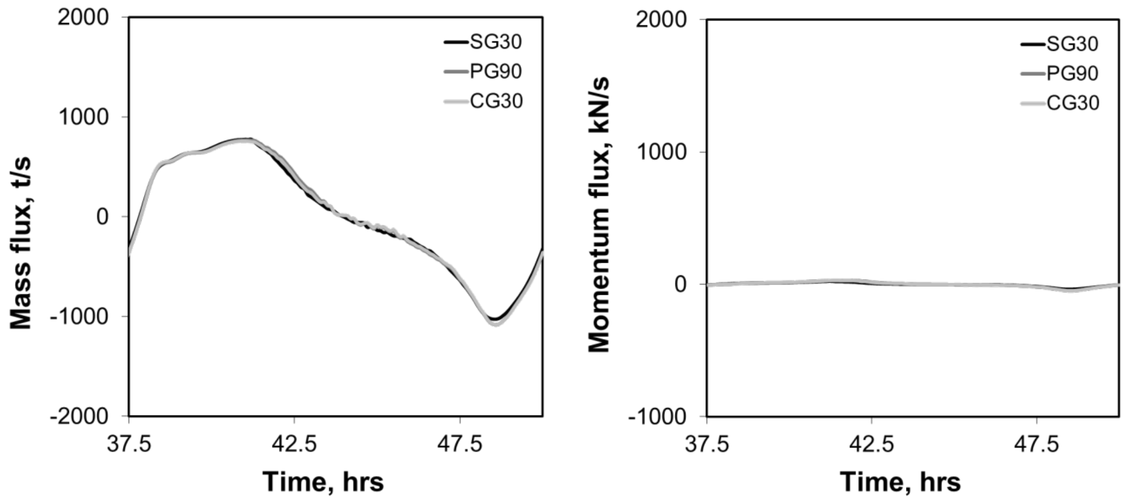

Figure 9: Comparison of (a) mass and (b) momentum fluxes across EB boundary; PG90 and CG30 timeseries are coincident.

(a) (b)

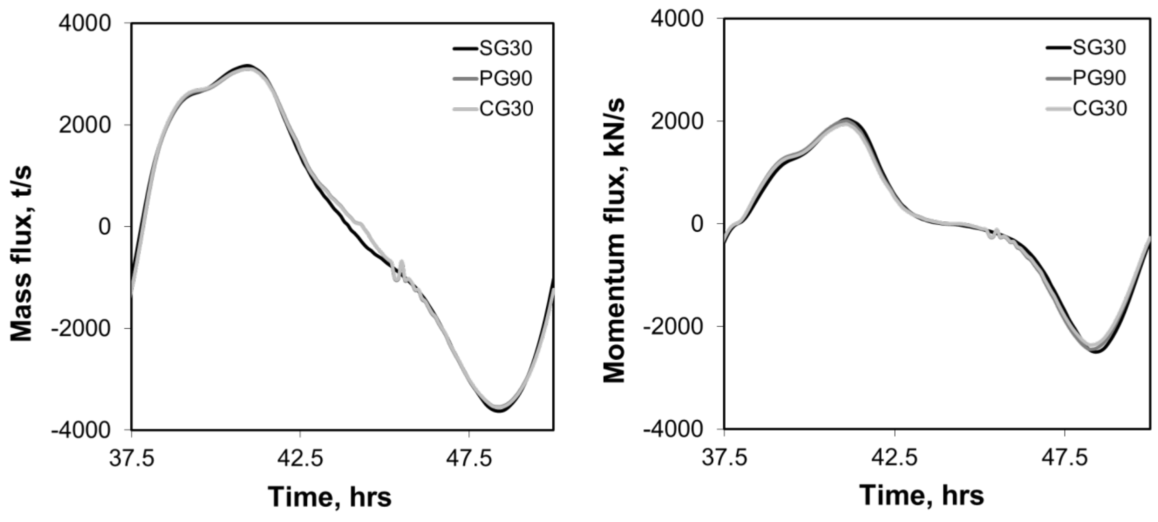

Figure 10: Comparison of (a) mass and (b) momentum fluxes across SB boundary; PG90 and CG30 timeseries are coincident.

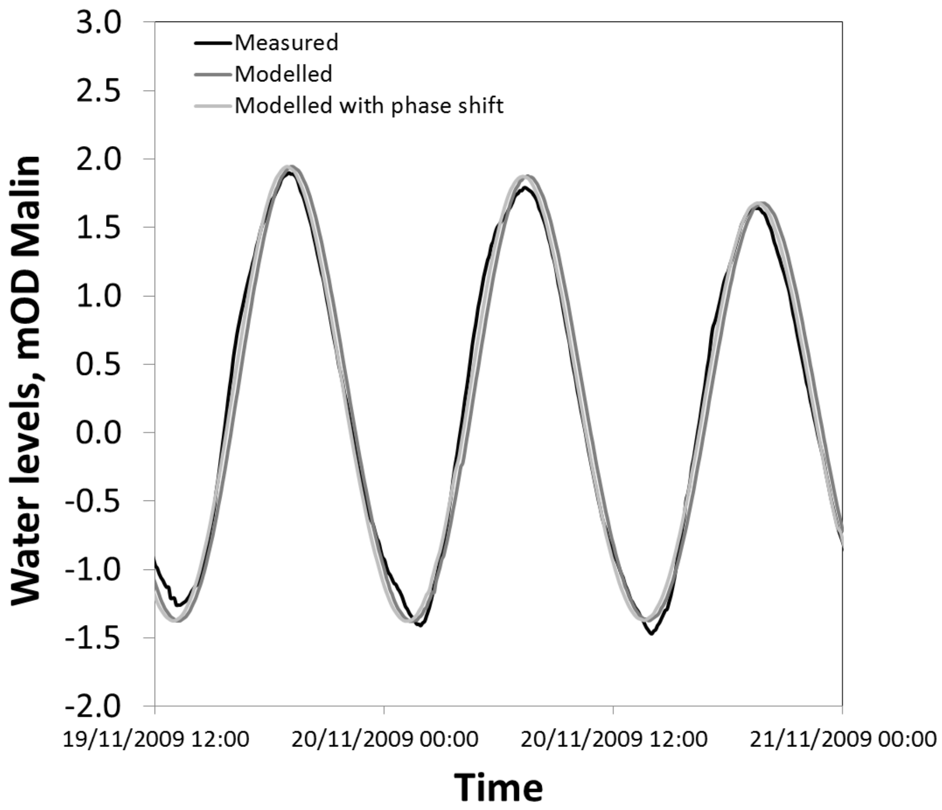

Figure 11: Water elevations modelled by CG06 and measured at Tivoli tidal gauge station.

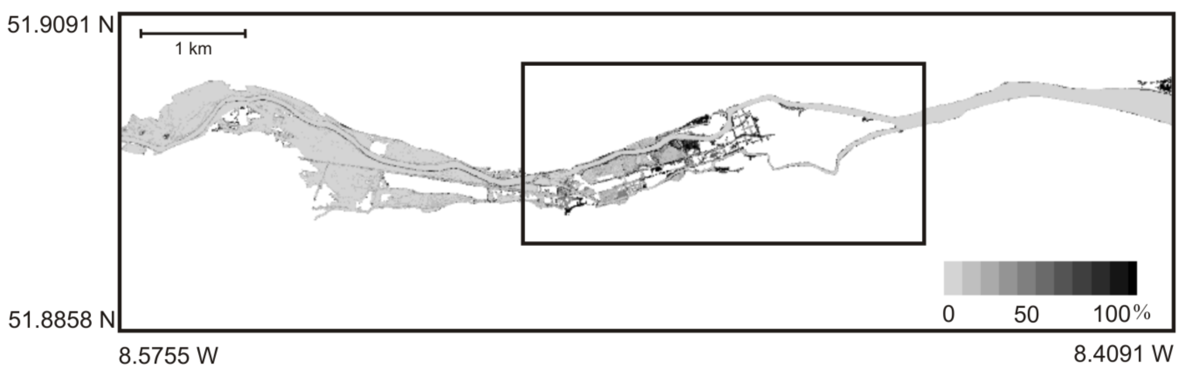

Figure 12: Water level RE_T (%) in CG06 relative to SG02 . Black box shows extent of CG02 and locations of nested boundaries.

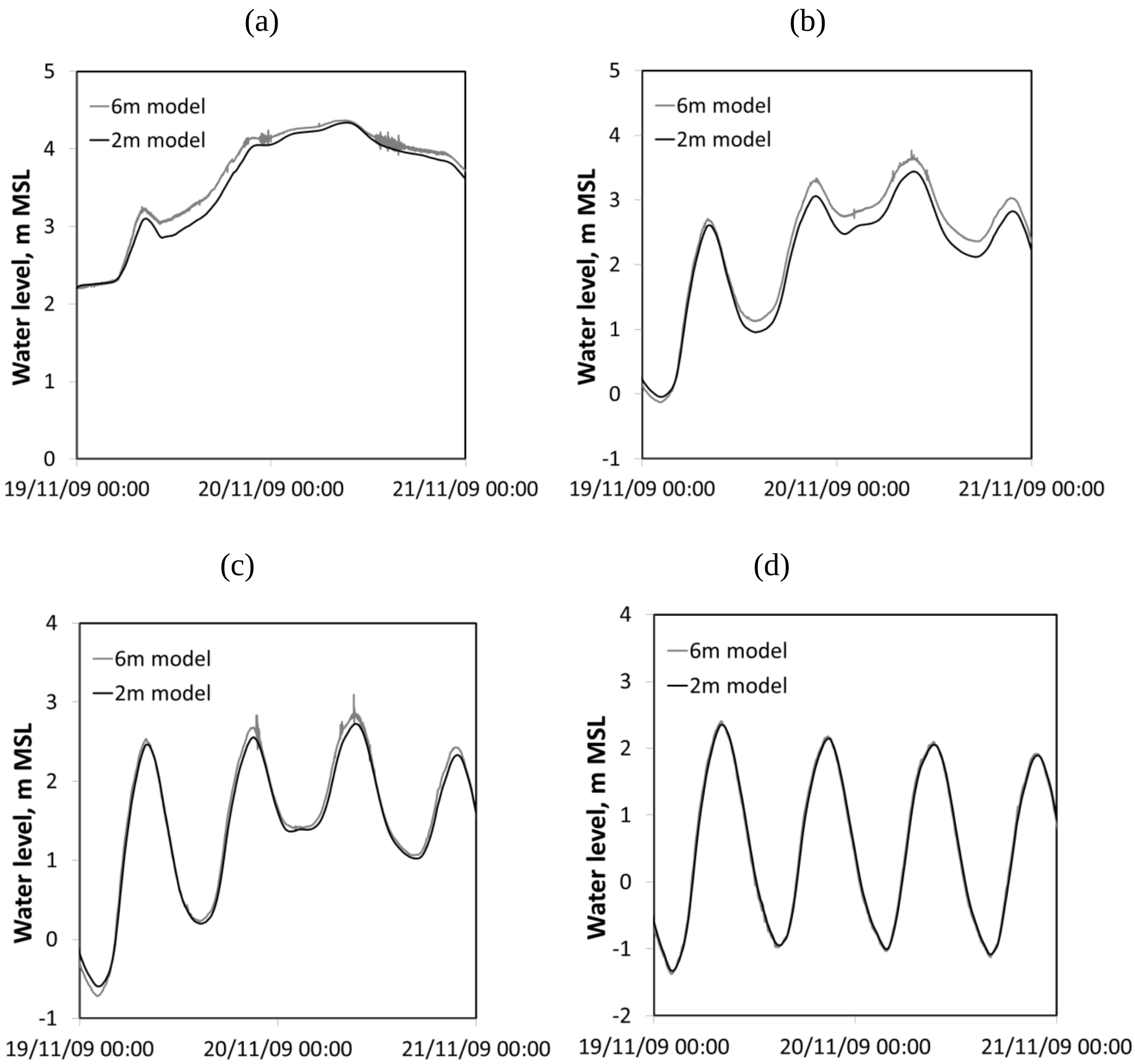

Figure 13: Timeseries of water elevations predicted by CG06 and CG02 at four locations (a) CG02_1, (b) CG02_2, (c) CG02_3, (d) CG02_4. Point locations shown in Fig. 14.

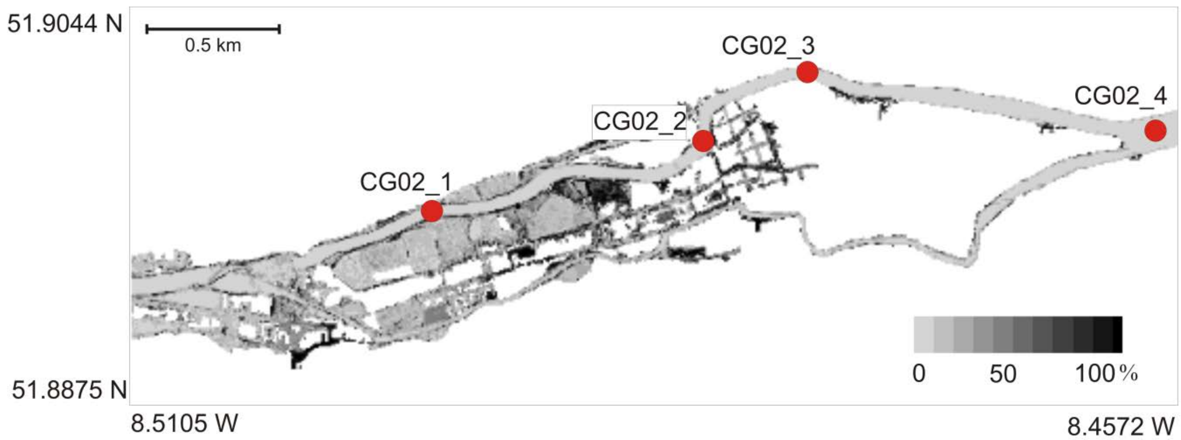

Figure 14: Water level RE_T (%) in CG02 relative to SG02 . Red dots denote points used in water level analysis (see Figure 13).

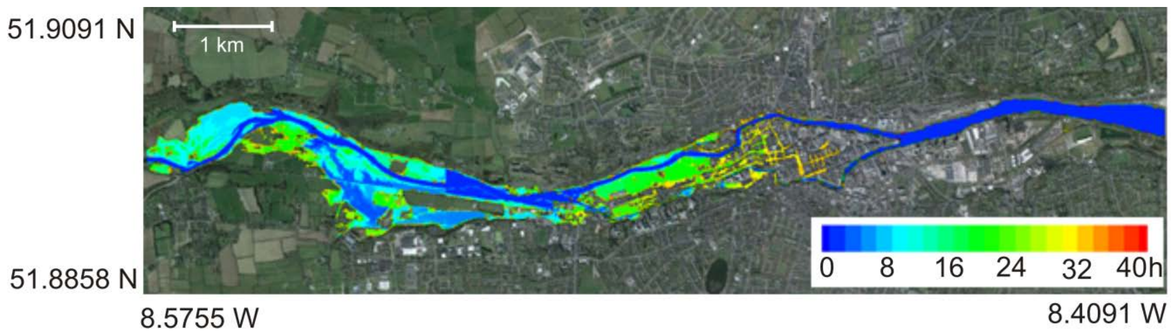

Figure 15: Temporal evolution of flood wave through upper and lower floodplains of Cork City during November 2009 flood event modelled by CG06; contours represent 2-h intervals.

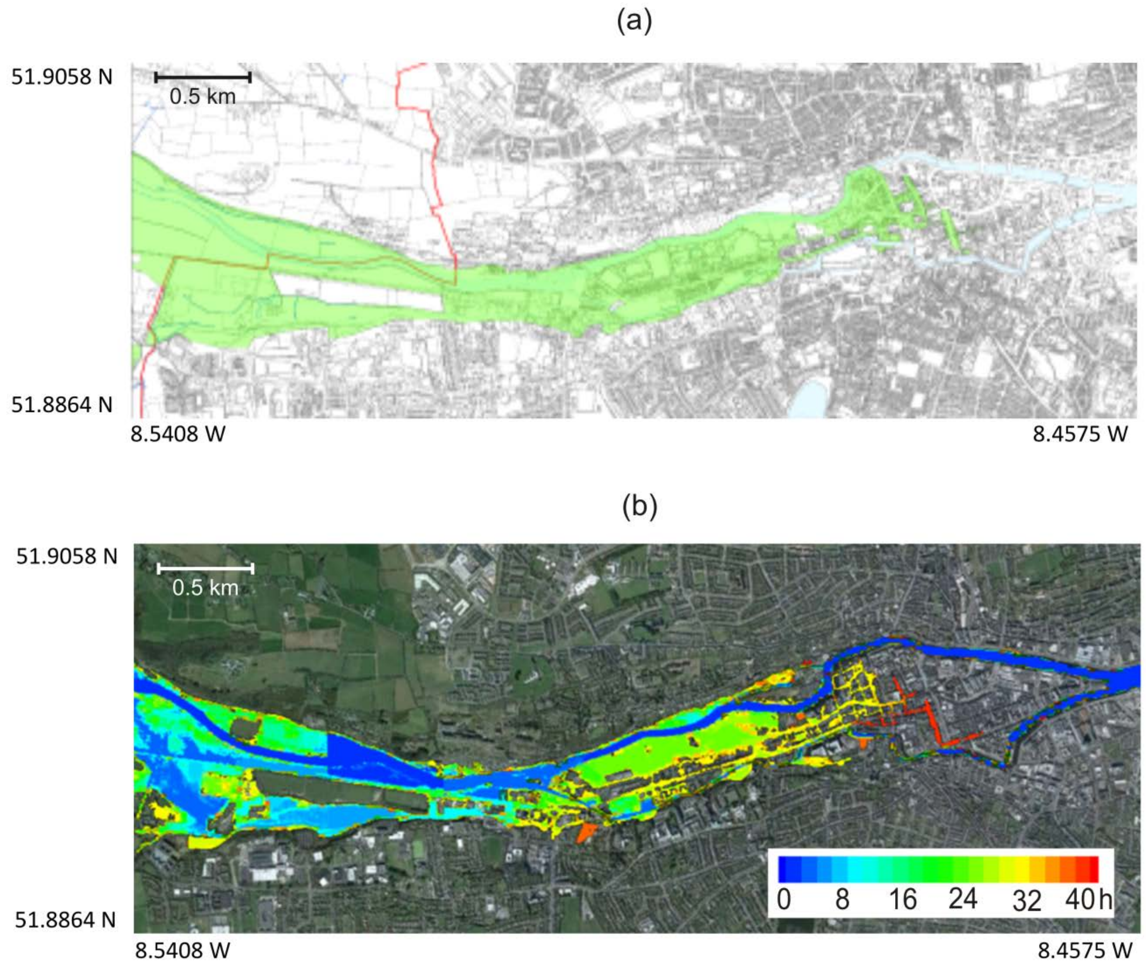

Figure 16: Maps of flood inundation (a) observed by OPW and (b) modelled; contours represent 2-h intervals. Evolution of modelled flood wave is a combined output of CG06 and CG02.

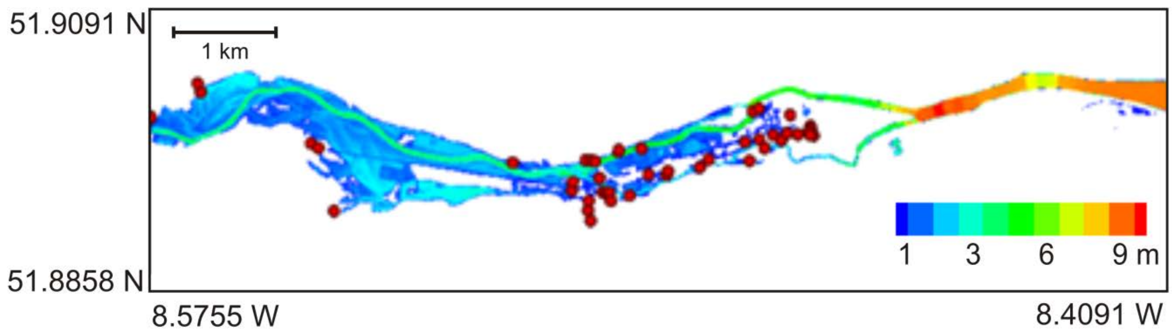

Figure 17: Maximum water levels during November 2009 flood event and water level survey points marked as red dots.

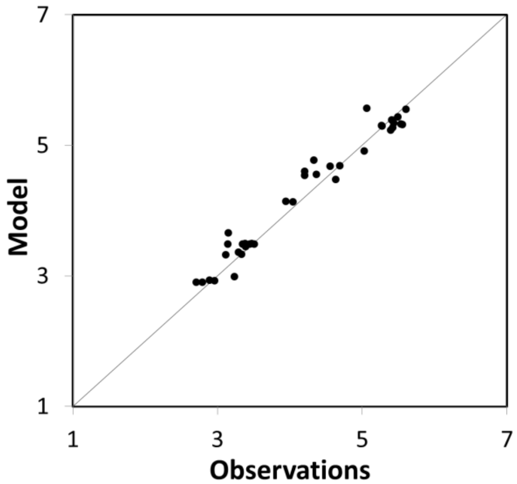

Figure 18: Comparison of modelled and observed maximum water elevations at 38 survey stations.

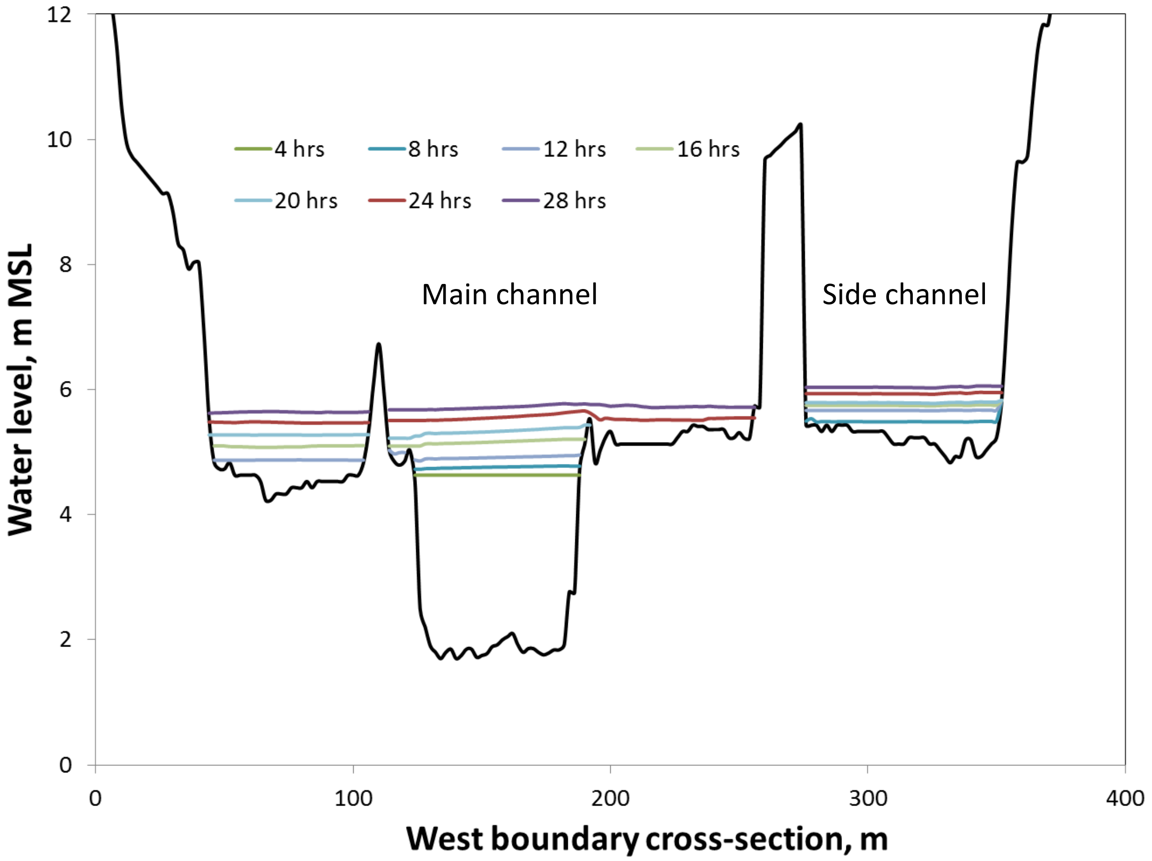

Figure 19: Cross-section through west boundary of CG02 with water elevation marks for selected time points.

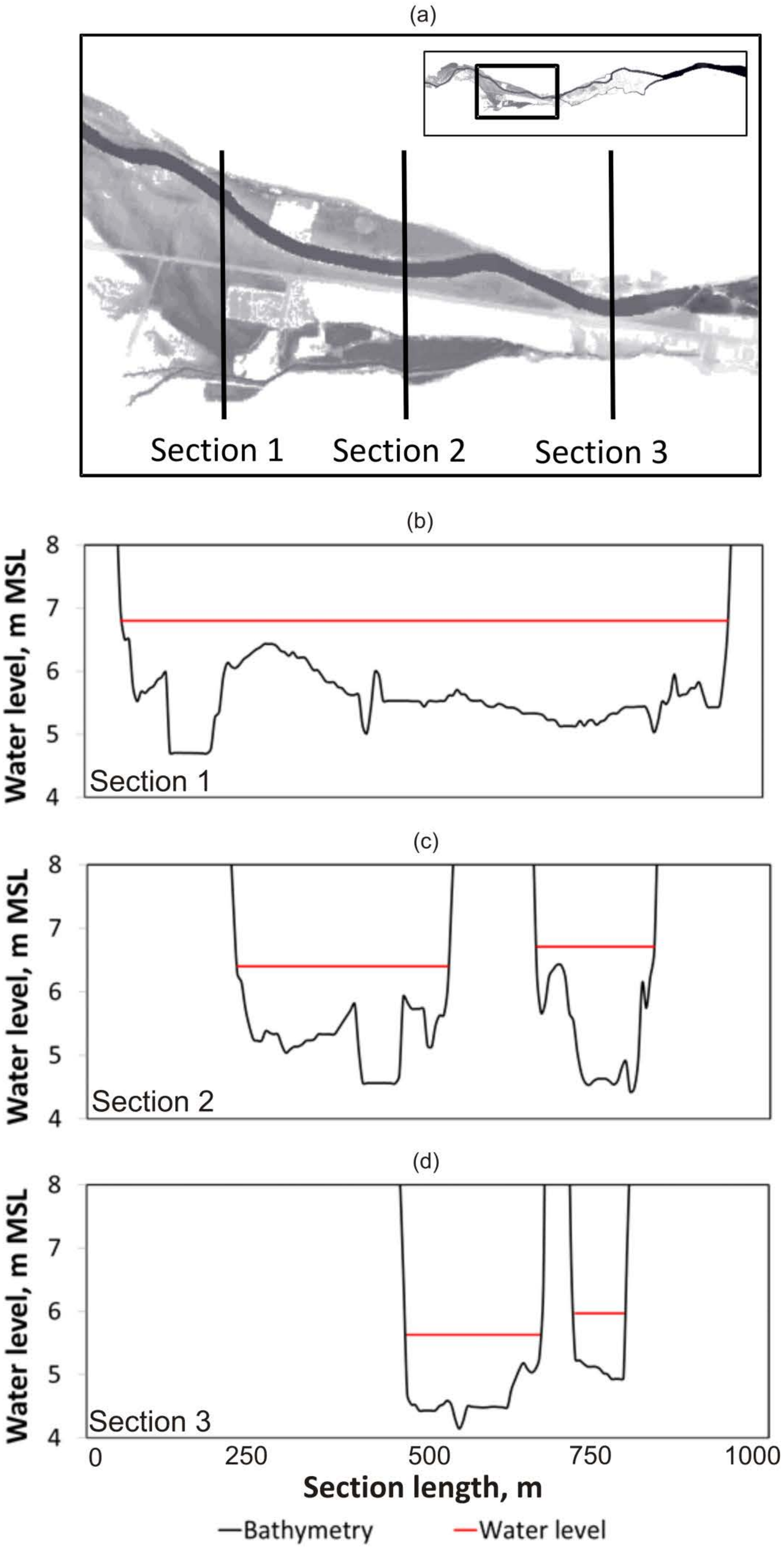
(a)
Section 1
Section 2
Section 3
(b)
Water level, m MSL
8
7
6
5
4
Section 1
(c)
Section 2
(d)
Section 3
0
250
500
750
1000
Section length, m
Bathymetry
Water level

979

Figure 20: (a) Flood extent in upper floodplains and (a-c) water elevations at three cross-sections during flood simulated by CG06.

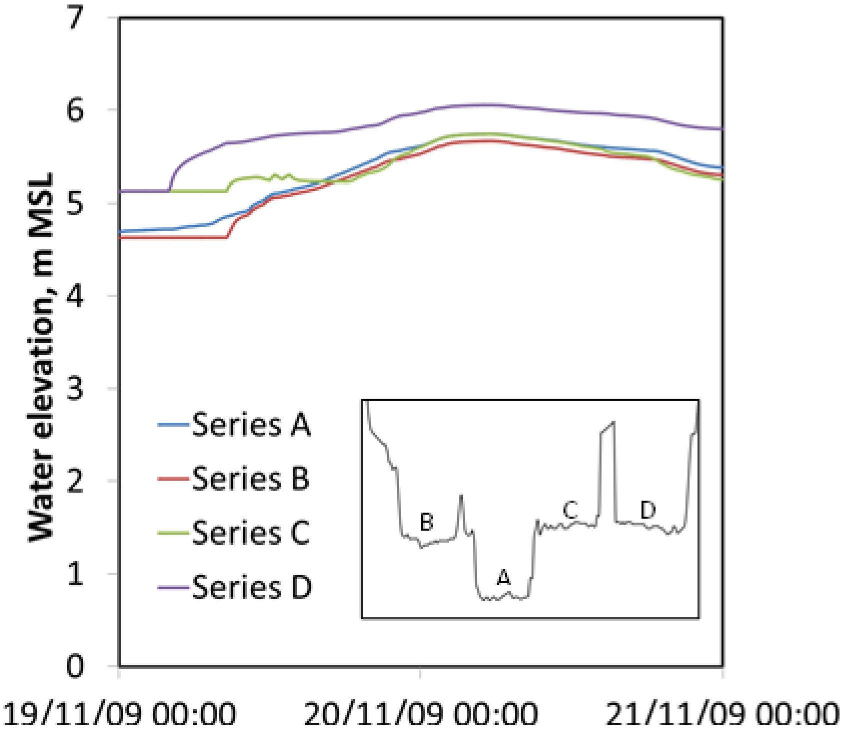

Figure 21: Timeseries of water elevations across the western nested boundary of CG02.

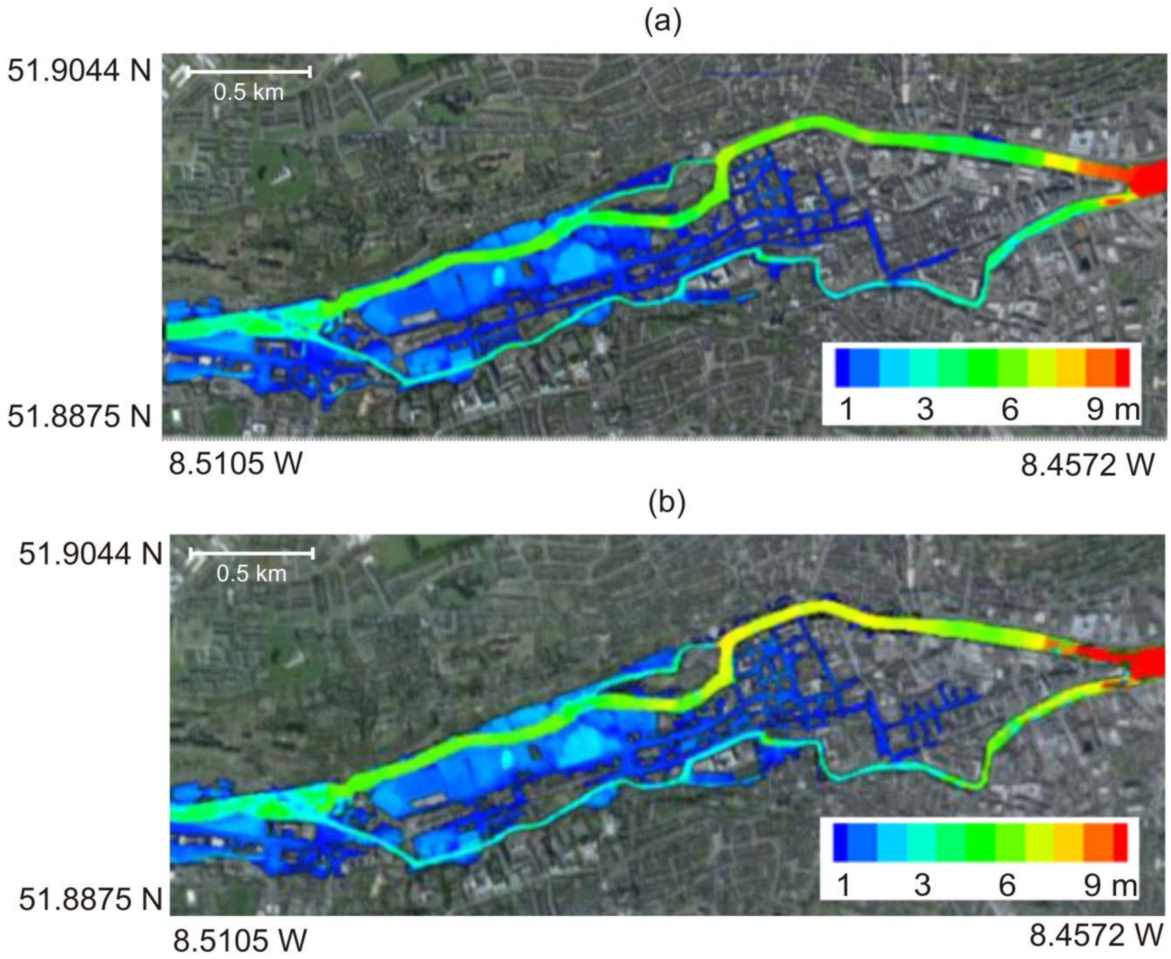

Figure 22: Comparison of flood extent simulated by (a) CG02 and (b) CG06. Contours represent water levels (m).

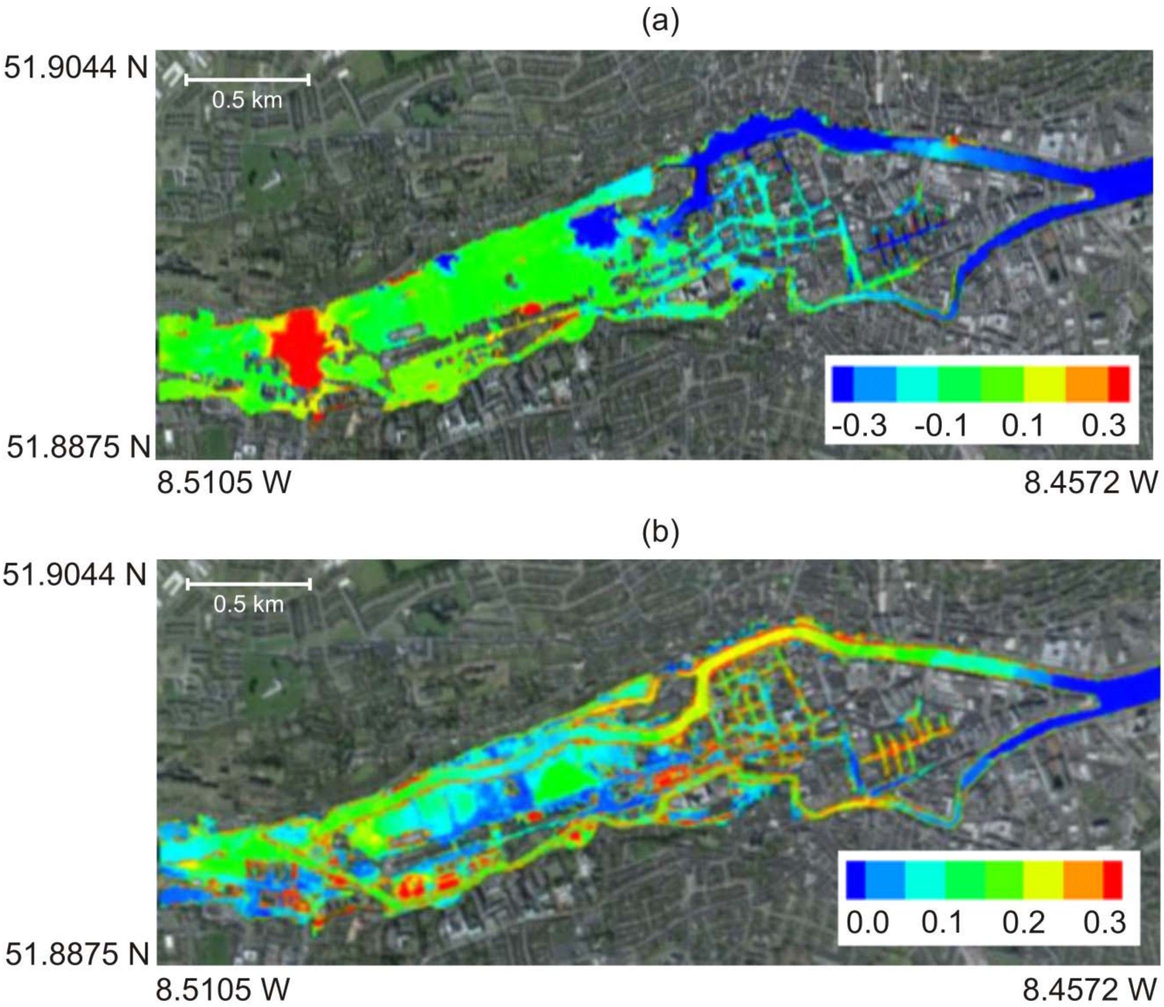

Figure 23: Contour plots of (a) difference in water elevations (m) between CG06 and CG02, and (b) RMSE over time.

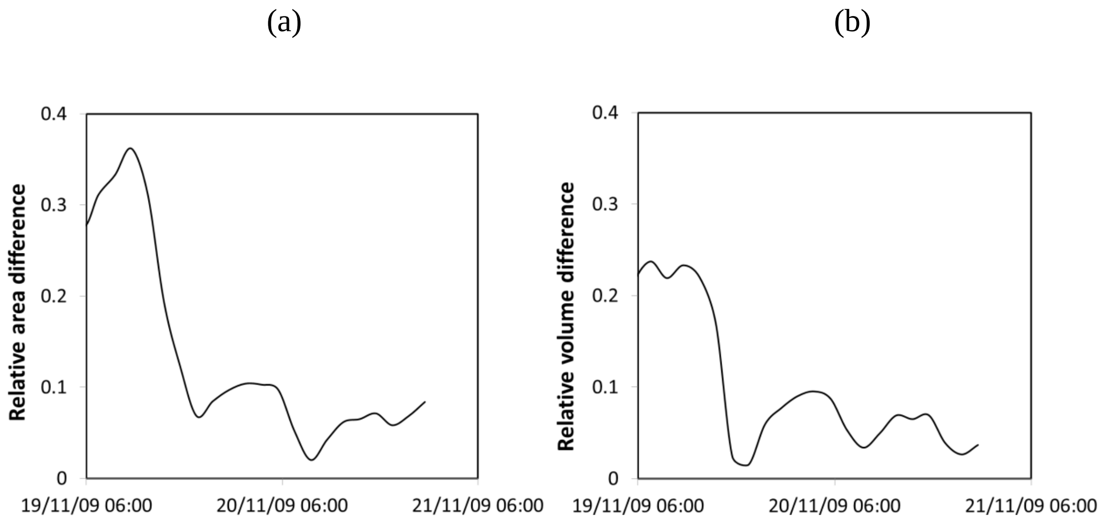

Figure 24: Evolution of the relative difference in (a) total area of inundation and (b) volume of water in inundated area between CG06 and CG02. See text for explanation of relative difference.

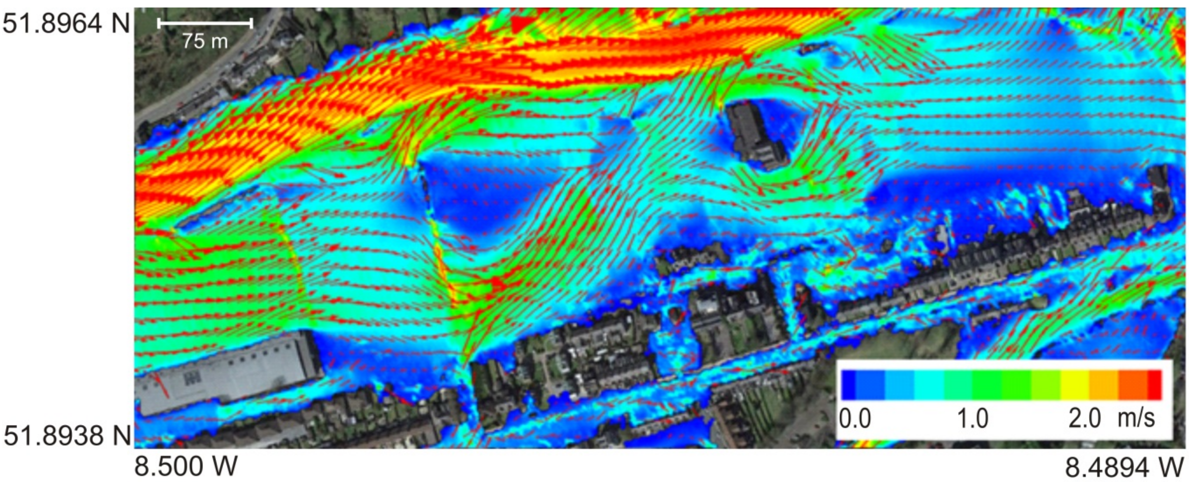

Figure 25: Map of velocity contours (m/s) with vectors showing magnitude and direction of velocities in the downstream floodplains of Cork City.